

# UC Berkeley

## UC Berkeley Previously Published Works

### Title

Estimation of Site Terms in Ground-Motion Models for California Using Horizontal-to-Vertical Spectral Ratios from Microtremor

### Permalink

<https://escholarship.org/uc/item/99d6w3gz>

### Journal

Bulletin of the Seismological Society of America, 112(6)

### ISSN

0037-1106 1943-3573

### Authors

Pinilla-Ramos, Camilo  
Abrahamson, Norman  
Kayen, Robert

### Publication Date

2024-07-31

### DOI

10.1785/0120220033

Peer reviewed

# Estimation of Site Terms in Ground-Motion Models for California Using Horizontal-to-Vertical Spectral Ratios from Microtremor

Camilo Pinilla-Ramos<sup>\*1</sup>, Norman Abrahamson<sup>1</sup>, and Robert Kayen<sup>1,2</sup>

## ABSTRACT

The horizontal-to-vertical spectral ratios from microtremor (mHVS<sub>R</sub>) data obtained at 196 seismic stations in California are used to evaluate three alternative microtremor-based proxies for site amplification for use in ground-motion models (GMMs): the site fundamental period ( $f_0$ ), the period-dependent amplitude of the mHVS<sub>R</sub>( $T$ ), and the normalized amplitude of the mHVS<sub>R</sub>( $T$ ). The alternative parameters are evaluated for the sites with and without measurements of  $V_{S30}$ . If a  $V_{S30}$  measurement is not available for a site, then  $f_0$  has the highest correlation with the site amplification for short periods ( $T < 1$  s) and the normalized amplitude of the mHVS<sub>R</sub>( $T$ ) has the highest correlation for long periods ( $T \geq 1$  s). If a measurement of the  $V_{S30}$  is available for a site, then the normalized amplitude of the mHVS<sub>R</sub>( $T$ ) has the highest correlation for the site amplification not explained by  $V_{S30}$  for all periods. For both cases, the correlations are strongest at the longer periods as mHVS<sub>R</sub>( $T$ ) measurements excel at providing valuable information for sites with long-period amplification due to the deeper velocity structure. In particular, for sites with a  $V_{S30}$  measurement, the normalized mHVS<sub>R</sub>( $T$ ) amplitude provides more information about the long-period site terms than the basin depth currently used in GMMs. Empirical models of the median and standard deviation of the site terms based on the normalized mHVS<sub>R</sub>( $T$ ) curves are developed for the two cases. These models can be used directly in the ASK14 GMM to modify the median and aleatory standard deviation or they can be used to estimate the site-specific site term in the context of a partially nonergodic GMM. Including the mHVS<sub>R</sub>( $T$ ) measurement can have a significant effect on estimates of the ground motion at a site: the range 5%–95% on the observed HVS<sub>R</sub>( $T$ ) values corresponds to factors of 0.6–1.6 for the median spectral acceleration for periods between 0.5 and 4 s.

## KEY POINTS

- Do HVS<sub>R</sub> measurements from microtremor improve the accuracy of site terms in ground-motion models in California.
- Microtremor HVS<sub>R</sub> provides useful constraints on the site terms either in addition to  $V_{S30}$ .
- HVS<sub>R</sub> from microtremor should be included as a site parameter in future ground-motion models.

## Supplemental Material

## INTRODUCTION

The linear site amplification for horizontal ground motion depends on the shear wave profile with depth,  $V_S(z)$ , and the low-strain damping. In ground-motion models (GMMs),

the full  $V_S(z)$  and damping profiles are commonly simplified to scalar parameters that can be used as input parameters in the regression. The most widely used site parameter in GMMs is  $V_{S30}$ , defined as the time-averaged shear-wave velocity over the top 30 m, but the  $V_{S30}$  is not a fundamental parameter for site amplification. There are multiple  $V_S(z)$  profiles that have the same  $V_{S30}$  but which have different site amplification; however,

1. Department of Civil Engineering, University of California, Berkeley, California, U.S.A., <https://orcid.org/0000-0002-4034-6618> (CP-R); <https://orcid.org/0000-0001-7900-6023> (NA); <https://orcid.org/0000-0002-0356-072X> (RK); 2. United States Geological Survey, Mountain View, California, U.S.A.

\*Corresponding author: [camilo.pinilla@berkeley.edu](mailto:camilo.pinilla@berkeley.edu)

**Cite this article as** Pinilla-Ramos, C., N. Abrahamson, and R. Kayen (2022). Estimation of Site Terms in Ground-Motion Models for California Using Horizontal-to-Vertical Spectral Ratios from Microtremor, *Bull. Seismol. Soc. Am.* **XX**, 1–21, doi: [10.1785/0120220033](https://doi.org/10.1785/0120220033)

© Seismological Society of America

$V_{S30}$  can be a useful parameter for estimating site amplification because, in natural deposits, the  $V_{S30}$  is often correlated with the deeper  $V_S$  profile that controls the site amplification (Boore *et al.*, 2011).

The Next Generation Attenuation (NGA)-West2 GMMs for California and Japan (Bozorgnia *et al.*, 2014) include a second site parameter based on the minimum depth to a  $V_S$  value of 1.0 km/s ( $Z_{1,0}$ ) or 2.5 km/s ( $Z_{2,5}$ ). The inclusion of an additional site term based on the depth to rock can improve the estimation of the long-period site amplification by distinguishing between shallow and deep soil sites with the same  $V_{S30}$ .

Another parameter that has been used for site classification in GMMs is the horizontal-to-vertical spectral ratio (HVSr) from earthquakes. For example, Zhao *et al.* (2006) used the period of the peak of HVSr ratio for 5%-damped pseudospectral acceleration (PSA) from earthquakes to classify strong-motion sites for development of a GMM for Japan. A similar approach was used by Di Alessandro *et al.* (2012) for Italian seismic stations and by Pinzón *et al.* (2019) for Spanish seismic stations. Mercado *et al.* (unpublished manuscript, 2021, see Data and Resources) extended this approach to include both the predominant period and the amplitude PSA HVSr from earthquakes to define the site classes for seismic stations in Colombia.

Using the HVSr from recorded earthquake ground motions to classify the site for use in developing a GMM has the drawback that it uses the observed horizontal ground motion in the HVSr to determine the site class used as an input parameter to the regression and as the horizontal ground-motion amplitude being modeled. Using the horizontal PSA values for both the determination of the input parameters and as the dependent variable being modeled can lead to an underestimation of the standard deviation of the resulting GMM. This circularity can be avoided using HVSr of the Fourier amplitude spectra (FAS) from microtremor (mHVSR) rather than from earthquakes (eHVSR) that are from the same set of earthquake recordings later used as the dependent parameter in the regression for the development of the GMM. In addition, defining a site term based on HVSr from earthquakes has the additional drawback that can be applied only to sites with available earthquake recordings, which is not practical for most projects; however, mHVSR measurements can be easily acquired at project sites.

### Use of microtremor data

Since the seminal work by Nakamura (1989), HVSr from microtremors has been used for site classification and site-effect evaluations in many parts of the world (e.g., Lachet *et al.*, 1996; Bonnefoy-Claudet *et al.*, 2006; Haghshenas *et al.*, 2008). Other studies have used HVSr for estimating the  $V_S$  profile and the site amplification for the horizontal component (e.g., Arai and Tokimatsu, 2004; Kawase *et al.*, 2011; Kawase, Nagashima, Nakano, and Mori, 2018). Recent reviews of the state-of-the-art using microtremor for site classification and characterization of site effects are given by Molnar *et al.*

(2016, 2022). A general result is that mHVSR is a good tool for identifying the fundamental frequency of sites with strong resonances and that the frequency identified from microtremor is similar to those from earthquakes inducing small strain regimes on the materials, which is approximately 0.05g peak acceleration (e.g., Satoh *et al.*, 2001; Rodriguez and Midorikawa, 2003; Cultrera *et al.*, 2014; Kawase, Mori, and Nagashima, 2018; Hassani *et al.*, 2019). In contrast, the amplitudes of the mHVSR are more variable than the fundamental frequency and are not as well understood. As a result, the main uses of mHVSR have been to estimate the fundamental frequency for site classification (e.g., Standards New Zealand [SNZ], 2004; Pitilakis *et al.*, 2018) and to screen candidate shear-wave velocity profiles for incorporation into site-specific ground response analyses, in which the mHVSR measurements can play a key role in establishing the experimental site signature (e.g., Teague *et al.*, 2018; Hallal and Cox, 2022).

In current GMMs that are widely used in seismic hazard practice in California, mHVSR has not been used for site classification or as a site parameter in the GMM. Part of the reason for this is that the velocity profiles for California strong-motion sites on soils tend to have velocity gradients rather than strong impedance contrasts, so there may not be a clear fundamental period in mHVSR data that are related to the site amplification. This is part of reason that  $V_{S30}$  was preferred as a site parameter for California GMMs starting in the 1990s.

Based on the similarity of the site fundamental period,  $f_0$ , estimated from earthquakes and microtremor, Hassani *et al.* (2019) suggested that the  $f_0$  estimated from mHVSR could be used as a continuous site parameter in GMMs, similar to the current use of  $V_{S30}$ . By continuous parameter on GMM, we mean a predictor that does not have categories and is a smooth transition in terms of site amplification. Using site terms estimated for California sites for a subset of the data used by Abrahamson *et al.* (2014) GMM (ASK14), we evaluate the predictive power of  $f_0$  as a continuous site parameter in a GMM framework as suggested by Hassani *et al.* (2019). To address the issue of velocity profiles in California being mainly gradients rather than strong impedance contrasts, we also consider the period-dependent amplitude of the entire mHVSR( $T$ ) curve as a continuous site parameter as an alternative to the fundamental period  $f_0$ . The advantage of using the amplitude is that it does not require identification of  $f_0$ , which can be difficult to determine for sites without strong resonances; however, the amplitude curve is less stable than the fundamental frequency  $f_0$  (Molnar *et al.*, 2022). The sensitivity of the mHVSR amplitude to the type of sensor used to obtain the mHVSR measurement and its coupling to the soil can be reduced using a normalized amplitude (Molnar *et al.*, 2022).

In this study, we evaluate the use of the  $f_0$  and mHVSR( $T$ ) amplitude, both normalized and unnormalized, as proxies for the site amplification for California sites, similar to the current use of  $V_{S30}$  as a proxy for site amplification. Our objective is to

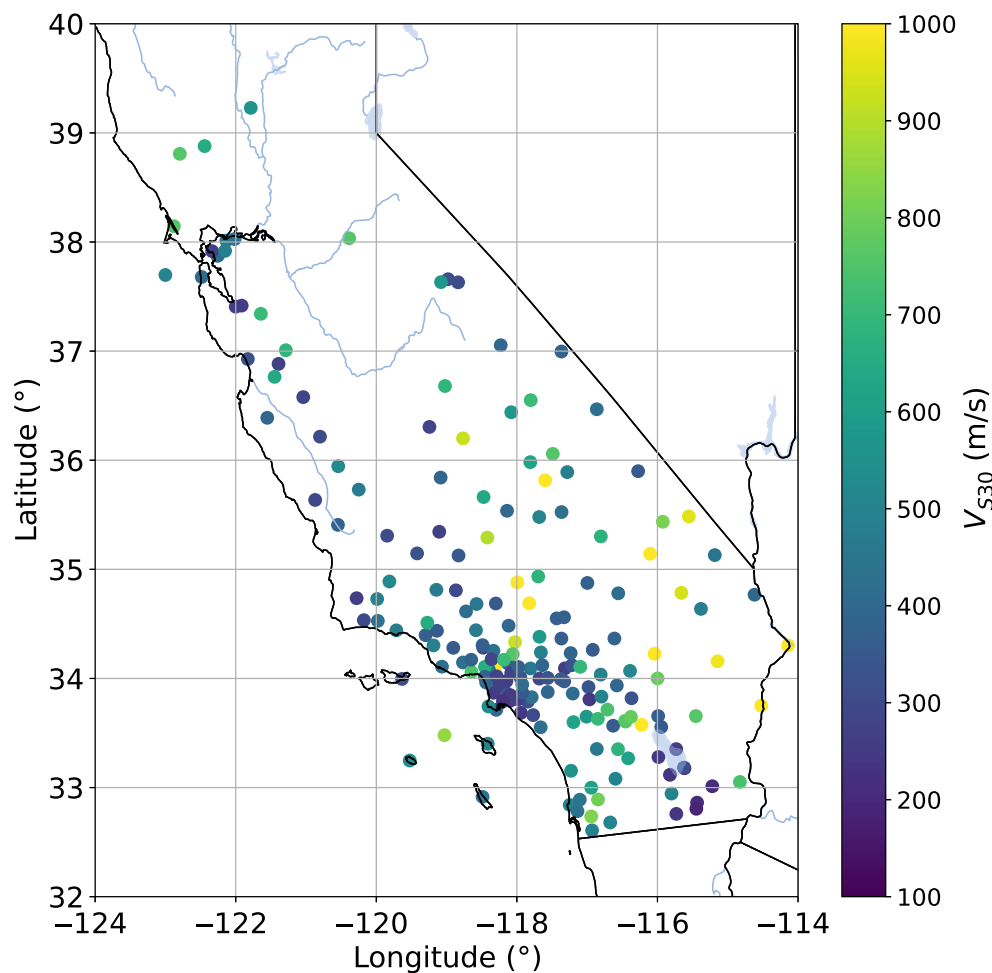


**Figure 1.** Locations of the stations in the selected dataset. The color version of this figure is available only in the electronic edition.

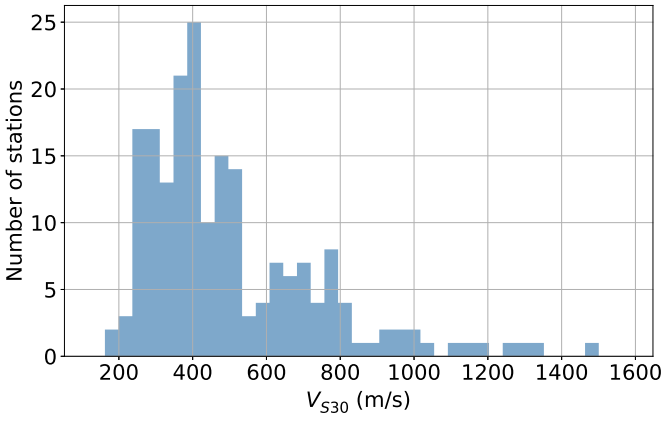


**Figure 2.** Distribution of  $V_{530}$  in the selected dataset. The color version of this figure is available only in the electronic edition.

determine if mHVSR data are useful site parameters for inclusion in future GMMs for use in California, either as an additional parameter to  $V_{530}$  or as a single parameter without  $V_{530}$ . To

the authors' knowledge, considering both  $V_{530}$  and mHVSR together has not been previously used in GMM. We do not address the physical theory behind the relation between mHVSR and site amplification; instead, we simply evaluate the usefulness of mHVSR-based site parameters as proxies for the site-specific site amplification. We show that the normalized HVSR( $T$ ) works better than either  $f_0$  or the unnormalized HVSR( $T$ ) for estimating the site amplification for California sites.

**GROUND-MOTION DATASET**

The empirical scaling with HVSR is derived from the residuals of the ASK14 GMM, based on the ground-motion dataset for California. We restricted the data to California sites because the correlation of the  $V_{530}$  and microtremor HVSR with the site amplification can vary by region. Combining data from multiple regions would obscure the effect of including microtremor HVSR as a site

parameter in regional GMMs. A subset of the ASK14 dataset was selected considering the following selection criteria: (1) the seismic station is located in California; (2) the station has recordings from at least three earthquakes to constrain the site term; (3) the station has continuous recordings that could be readily downloaded for a noise sample; and (4) the station has three components that are reliable. There were 746 stations that met the first two criteria of which 214 had continuous data that were accessible for automated downloading using the open-source ObsPy module for Python (Beyreuther *et al.*, 2010). A total of 18 stations were discarded as being unreliable based on inconsistencies in the phasing of the waveforms between the three components. The final ground-motion dataset used in this study includes a total of 5797 recordings from 196 stations and is given in the supplemental material available to this article.

The locations of the selected 196 stations in California are shown in Figure 1. The  $V_{530}$  values are taken from the NGA-W2 dataset. The distribution of the  $V_{530}$  for the selected set of sites (Fig. 2) shows that there is a good sampling of the  $V_{530}$  values between 300 and 800 m/s, but there are only nine sites

Downloaded from <http://pubs.geoscienceworld.org/ssa/bssa/article-pdf/doi/10.1785/0120220033/5719220/bssa-2022033.1.pdf> by USGS Library user

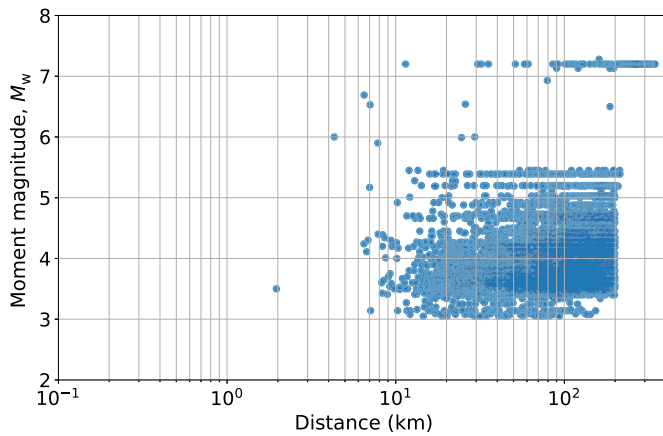


**Figure 3.** Magnitude–distance distribution of the selected dataset. The color version of this figure is available only in the electronic edition.

with  $V_{S30}$  over 1000 m/s. The distribution of magnitudes and distances is shown in Figure 3. Most of the recordings are from  $M$  3.5 to 5.0 earthquakes. These small magnitude events are included to have enough data to constrain the site term, but by using weak motion from small magnitudes, only the linear site term can be estimated. The nonlinear site terms need to be constrained by strong ground motions or analytical modeling.

The usable bandwidth for each recording is given in the NGA-W2 dataset (Ancheta *et al.*, 2014). The spectral accelerations are only used for spectral periods up to the longest usable period for each recording. As a result, the number of recordings changes as a function of period. The distributions of the number of recording per site that are reliable at a given period are shown in Figure 4. The distributions are shifted to fewer recording per station as the period increases with the largest reductions in usable data at periods greater than 1.5 s.

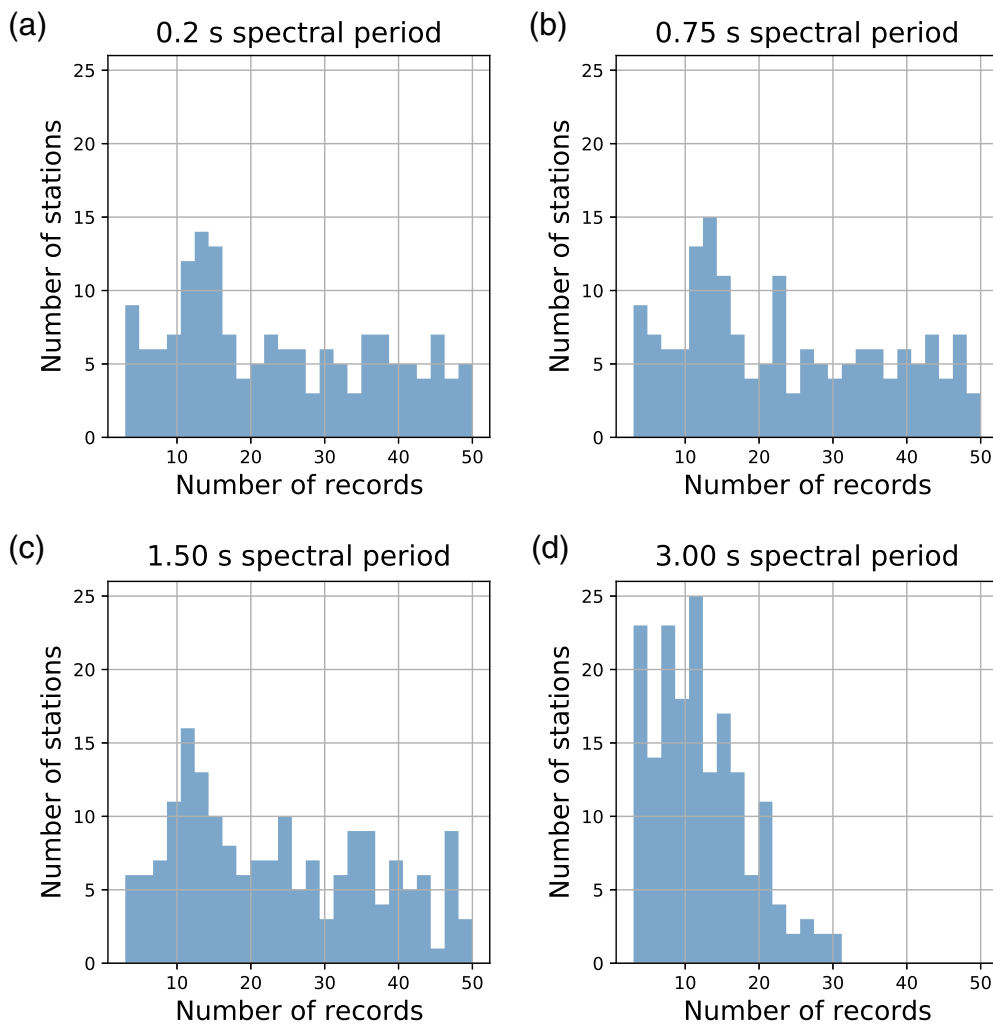


**Figure 4.** This figure shows the period-dependent number of stations with usable number of records in the selected dataset for four spectral periods: (a)  $T = 0.2$  s, (b)  $T = 0.75$  s, (c)  $T = 1.5$  s, and (d)  $T = 3$  s. The horizontal axis shows the number of records that are considered reliable for a given spectral period. The vertical axis shows the number of stations that have a given number of reliable records. The color version of this figure is available only in the electronic edition.

### MICROTREMOR SIGNAL PROCESSING

For each station with continuous data, a 60 min sample of the ambient noise was downloaded. The standard deviation of the HVSR from microtremors is larger during the day than during the night when local cultural noise is reduced. Therefore, the samples of the microtremors were obtained during the night: specifically between 2 a.m. and 3 a.m. local time.

The data were processed using the [Site EffectS Assessment using Ambient Excitations \(SESAME\) Project \(2004\)](#) procedure and criteria. The signal processing steps applied to the microtremors data to obtain the HVSR estimates are given subsequently:

- Divide the 60 min recording into 40 s time samples.
- Apply a 5%-cosine bell taper to each 40 s section.
- Compute the Fourier transform of the windowed data.
- Smooth the FAS with a Konno–Ohmachi window (Konno and Ohmachi, 1998) with a smoothing parameter of  $b = 40$ , as recommended by Cox *et al.* (2020).

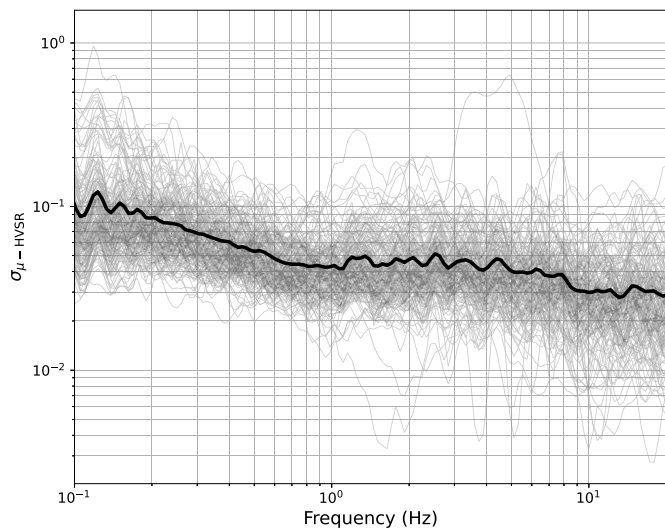


**Figure 5.** Standard error of the mean horizontal-to-vertical spectral ratio (HVSR) as a function of frequency for all the stations. The black line corresponds to the geometric mean for all sites together.

- Compute the mHVSR for each horizontal component for each 40 s time sample.
- Compute the geometric mean mHVSR over the ninety 40 s time samples for each component.
- Compute the geometric mean of mHVSR for the two horizontal components from the previous step.

The standard error of the mean  $\ln(\text{mHVSR}(T))$  computed from the ninety 40 s time windows is shown in Figure 5 for every station, as well as the geometric mean for all the stations together (the black line). On average, the standard error ranges from 0.04 to 0.1 which is much smaller than the range of  $\ln(\text{mHVSR}(T))$ , indicating that the mHVSR values are stable.

An initial evaluation showed that the correlation between the  $\text{mHVSR}(T)$  and the site amplification was improved if the  $\text{mHVSR}(T)$  was normalized by the geometric mean  $\text{mHVSR}(T)$  over 0.25–15 Hz using equally spaced frequencies on a log scale. The normalized  $\text{mHVSR}(T)$ , denoted  $\text{mHVSR}^*(T)$ , is given by:

$$\text{mHVSR}^*(T) = \frac{\text{mHVSR}(T)}{\overline{\text{mHVSR}[0.25-15 \text{ Hz}]}}. \quad (1)$$

The normalization factor is given by:

$$\begin{aligned} & \overline{\text{mHVSR}[0.25-15 \text{ Hz}]} \\ &= \left( \prod_{i=1}^{N_f} \text{mHVSR}(T_i) \right)^{1/N_f}, \end{aligned} \quad (2)$$

in which  $N_f$  is the number of frequencies between 0.25 and 15 Hz; we used  $N_f = 43$ .

Examples of the mHVSR from this dataset are shown in Figure 6. One site has a clear peak in the mHVSR, but the other two sites do not show a clear peak. Without a clear  $f_0$ , the mHVSR amplitude can still be used as an input parameter for the GMM.

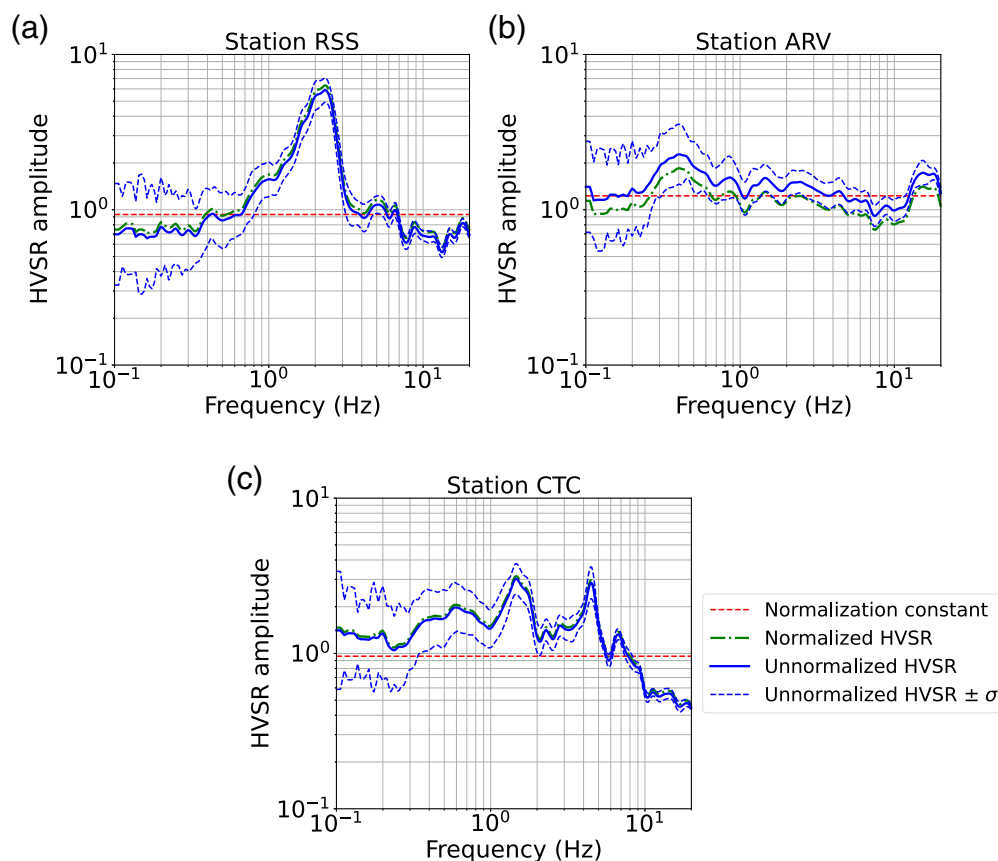


**Figure 6.** Example of the horizontal-to-vertical spectral ratio from microtremor (mHVSR) for three sites: (a) Station RSS, (b) Station ARV, and (c) Station CTC. For stations RSS and CTC, the normalization constant is almost 1.0. Therefore, the normalized and the unnormalized HVSR are almost identical. The color version of this figure is available only in the electronic edition.

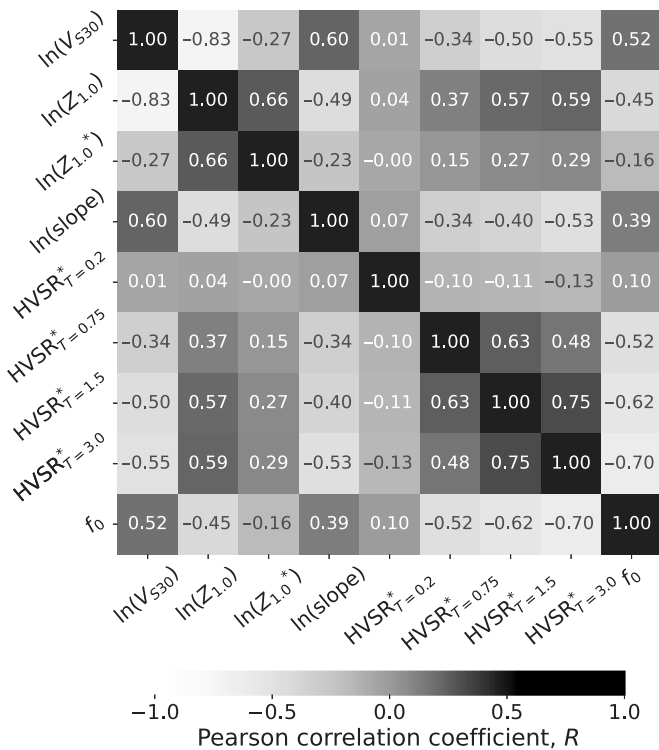


**Figure 7.** Correlation matrix for mHVSr parameters and the commonly used site parameters  $V_{S30}$  and  $Z_{1.0}$ . The  $Z_{1.0}^*$  corresponds to the normalized  $Z_{1.0}$  as defined by Abrahamson *et al.* (2014).

of 0.2, 0.75, 1.5, and 3 s) is shown in Figure 7. For the basin depth term, the correlation is shown for both  $Z_{1.0}$  and the normalized  $Z_{1.0}^*$  given by:

$$Z_{1.0}^* = \frac{Z_{1.0} + 0.01}{Z_{1.0-ref}(V_{S30}) + 0.01}, \quad (3)$$

in which  $Z_{1.0}$  is in km and  $Z_{1.0-ref}(V_{S30})$  is the median  $Z_{1.0}$  for the  $V_{S30}$  of the site. As shown in Figure 7, using the normalized  $Z_{1.0}^*$  reduces the correlation between the basin depth and the  $V_{S30}$  from  $-0.83$  to  $-0.27$ . A smaller correlation between the predictors is desirable, as it reduces the trade-off in the estimated regression coefficients. This normalized basin depth term is used in the ASK14 GMM.

None of the  $V_{S30}$  values in the NGA-W2 dataset for California were estimated from correlations with topographic slopes, but in other datasets, the topographic slope is sometimes used as a proxy for  $V_{S30}$ . In our dataset, there is a significant correlation between  $\ln(\text{slope})$  and the  $\ln(V_{S30})$ : correlation coefficient of  $-0.60$ . In the evaluation of the site parameters, we include the  $\ln(\text{slope})$  as a parameter for estimating the site term directly rather using the slope to estimate the  $V_{S30}$  for evaluating the predicting power of the slope on the site term as compared to the  $V_{S30}$  value.

The absolute value of the correlation between  $\ln(V_{S30})$  and  $\ln(\text{mHVSr}(T)^*)$  increases for longer periods, with correlations of about  $-0.55$  at periods of 1.5–3 s. The correlation between

$\ln(V_{S30})$  and  $\ln(\text{mHVSr}(T)^*)$  is negative because the ground-motion amplitude decreases with increasing  $V_{S30}$  but increases with increasing  $\text{mHVSr}(T)^*$ . The large negative correlation at long periods indicates that some of the  $V_{S30}$  scaling at long periods can be captured by a site-specific measurement of  $\text{mHVSr}^*$  if a site-specific estimate of  $V_{S30}$  is not available.

The correlation between  $f_0$  and  $\ln(V_{S30})$  is 0.42. The positive correlation is expected because softer sites will tend to have lower fundamental frequencies. The correlation between  $f_0$  and  $\ln(\text{mHVSr}^*)$  is negative and its absolute value increases for longer periods, indicating that the  $f_0$  is a better predictor of the mHVSr amplitude at long periods than at short periods.

## SITE TERMS

The residuals of the selected subset relative to the ASK14 GMM are computed using two random effects: one for the earthquake and one for the site. Using the notation of Al-Atik *et al.* (2010), the PSA from earthquake  $e$  recorded at station  $s$  is written as:

$$\ln(\text{PSA}_{es}) = \text{ASK14}(M, R_{rup}, V_{S30}, Z_{1.0}, \dots) + a_1 + \delta S_2 S_s + \delta W S_{es} + \delta B_e, \quad (4)$$

in which  $\text{ASK14}(M, R_{rup}, V_{S30}, Z_{1.0}, \dots)$  is the median estimate from the ASK14 GMM,  $\delta B_e$  is the between-event residual,  $\delta S_2 S_s$  is the between-site residual, and  $\delta W S_{es}$  is the within-site residual.  $\delta S_2 S_s$  is also called the site term. The  $a_1$  term represents the mean difference between our dataset and the full NGA-W2 dataset for California. The constant is needed so that the residuals terms have mean 0.

$\delta W S_{es}$  represents the variations in the distance scaling (geometrical spreading and anelastic attenuation,  $Q$ , terms) as well as azimuthally dependent variations in the source, path, and site effects. The standard deviations of  $\delta B_e$ ,  $\delta S_2 S_s$ , and  $\delta W S_{es}$  are denoted  $\tau$ ,  $\phi_{S_2 S_s}$ , and  $\phi_{S S_s}$ , respectively. In the ASK14 GMM, the site term is relative to the site with  $V_{S30} = V_{lin}$  and given by two terms:

$$\frac{\text{PSA}(V_{S30}, Z_{1.0})}{\text{PSA}(V_{lin})} = f_5(V_{S30}, \text{PSA}_{1100}) + f_{10}(Z_{1.0}, V_{S30}), \quad (5)$$

in which the  $f_5$  term gives the amplification relative to a reference  $V_{S30} = V_{lin}(T)$  and is dependent on the  $V_{S30}$  and the median PSA for  $V_{S30} = 1100$  m/s ( $\hat{\text{PSA}}_{1100}$ ) for nonlinear site effects. The  $f_{10}$  term gives the basin term relative to the average  $Z_{1.0}$  for the given  $V_{S30}$ .

## Evaluations of parameters for the total site terms

For the initial evaluation of the alternative mHVSr-based site parameters as proxies for the site amplification, the site-specific site terms are first computed by removing the  $V_{S30}$  and  $Z_{1.0}$  scaling in the ASK14 GMM as shown in equation (6). The resulting site terms reflect the total site amplification

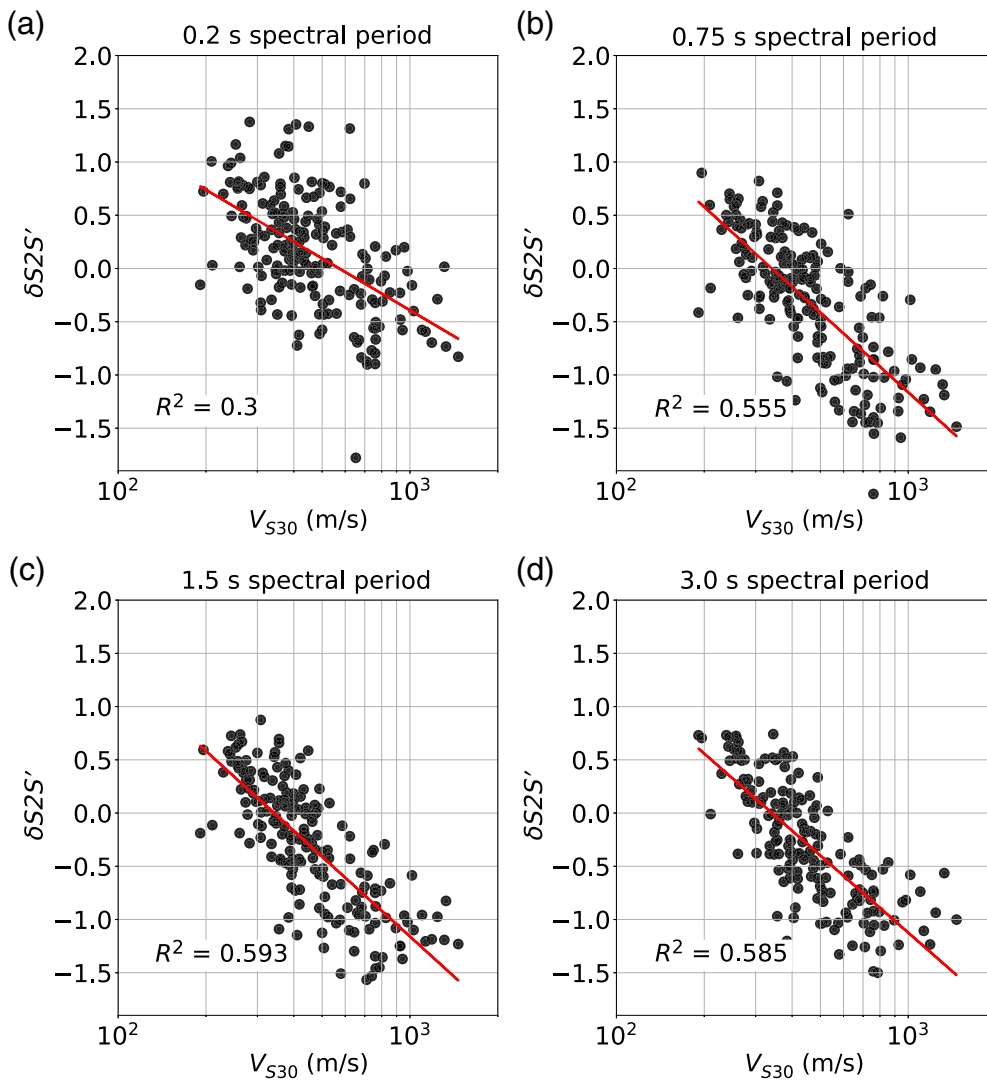


**Figure 8.** Scatter plot showing the correlation of the site terms without the ASK14 site factors,  $\delta S2S'$ , and the  $\ln(V_{S30})$  for four spectral periods for the selected dataset of sites in California: (a) 0.2 s spectral period, (b) 0.75 s spectral period, (c) 1.5 s spectral period, and (d) 3.0 s spectral period. The color version of this figure is available only in the electronic edition.

relative to  $V_{S30} = V_{lin}$ , not just the difference from the site scaling in the GMM. This total site term is denoted  $\delta S2S'_s$ :

$$\begin{aligned} \ln(\text{PSA}_{es}) = & [\text{ASK14}(M, R_{rup}, V_{S30}, Z_{1.0}, \dots) \\ & - f_5(V_{S30}, \text{PSA}_{1100}) - f_{10}(Z_{1.0}, V_{S30})] \\ & + a_1 + \delta S2S'_s + \delta WS_{es} + \delta B_e. \end{aligned} \quad (6)$$

Examples of the correlation of  $\delta S2S'$  with the  $\ln(V_{S30})$ ,  $\ln(Z_{1.0})$ ,  $f_0$ , and  $\ln(\text{mHVSR}^*(T))$  are shown in Figures 8–11, respectively, for periods of 0.2, 0.75, 1.5, and 3 s. The correlation with unnormalized  $\ln(\text{mHVSR})$  is similar to that for the normalized  $\ln(\text{mHVSR}^*)$  (not shown). For  $f_0$ , only a subset of 90 stations that satisfy five out of the six [SESAME Project \(2004\)](#) criteria for a reliable  $f_0$  are used, out of the total of 196 stations. The correlation with  $\ln(V_{S30})$  shown in Figure 8 describes how

well the  $\ln(V_{S30})$  site parameter predicts the actual site term for California sites. Figures 9–11 show how well the other site parameters predict the site term if  $V_{S30}$  was not used. All of the site parameters show stronger correlation with  $\delta S2S'$  at the longer periods. The trend of increasing correlation of the mHVSR amplitude with longer period is consistent with the results of [Najafomarei et al. \(2020\)](#) which showed a stronger correlation between the ground-motion amplitude and mHVSR for spectral periods over 0.5 s than for the shorter spectral periods.

The correlation of each parameter with the observed site amplification is measured by the  $R^2$ . The period dependence of  $R^2$  for each site parameter is shown in Figure 12. The  $R^2$  values for  $\ln(Z_{1.0})$  have a similar period dependence as for  $\ln(V_{S30})$  as a result of the high correlation between  $\ln(V_{S30})$  and  $\ln(Z_{1.0})$  (correlation coefficient  $R = -0.83$ ). The  $R^2$  values for the unnormalized  $\ln(\text{mHVSR}(T))$  are much smaller than for the normalized  $\ln(\text{mHVSR}^*)$  for period between 0.3 and 2 s. The  $R^2$  values for  $f_0$  are larger than for  $\ln(\text{mHVSR}^*)$  for periods of 0.25–0.75 s, but they are lower than  $\ln(\text{mHVSR}^*)$  at periods greater than 1 s.

Overall, the  $R^2$  values shown in Figure 12 indicate that  $\ln(V_{S30})$  is a much better predictor of site amplification than  $\ln(\text{mHVSR}^*)$  at short and intermediate periods, but they become more similar as the period increases. This comparison shows that while the  $f_0$  and the  $\text{mHVSR}^*(T)$  does not predict site amplification for California sites as well as  $V_{S30}$ , they do provide useful information on the site amplification, particularly for periods greater than 0.5 s. These results apply only to California sites. For sites in other regions with strong site resonances, the parameter that has the highest correlation with the site terms may be different. For example, in regions with strong site resonances, the  $f_0$  may be a better parameter than  $V_{S30}$  for estimating the site terms.



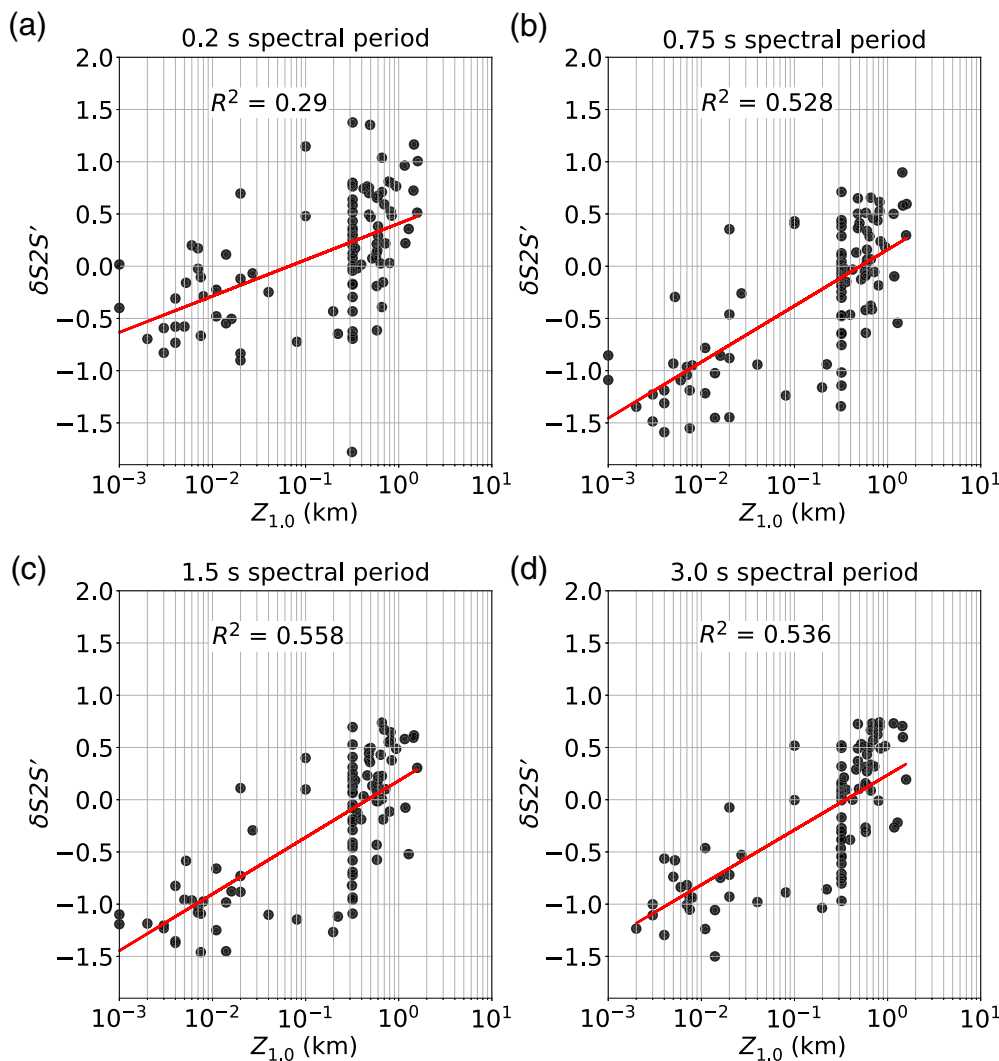


**Figure 9.** Scatter plot showing the correlation of the site terms without the ASK14 site factors,  $\delta S2S'$ , and the  $\ln(Z_{1.0})$  for four spectral periods: (a) 0.2 s spectral period, (b) 0.75 s spectral period, (c) 1.5 s spectral period, and (d) 3.0 s spectral period. This subset only includes 106 stations that have  $Z_{1.0}$  values in the Next Generation Attenuation-West2 (NGA-W2) dataset. The color version of this figure is available only in the electronic edition.

### Evaluations of parameters for the relative site amplification

The site terms are also computed relative to the  $V_{S30}$  scaling in the ASK14 GMM ( $\delta S2S$ ) using the default values for  $Z_{1.0}$  for the site  $V_{S30}$ . The dependence of the relative site term,  $\delta S2S$ , on the  $\ln(\text{mHVSR}^*)$  is shown in Figure 13. The correlation is reduced compared to the case without  $V_{S30}$  shown in Figure 11 due to the correlation between  $\ln(V_{S30})$  and  $\ln(\text{mHVSR}^*)$ . If the two parameters were perfectly correlated, then the fit to  $\ln(V_{S30})$  would explain all of the scaling with  $\ln(\text{mHVSR}^*)$  and the  $R^2$  values for the relative site term would be zero. Because these two parameters are partially correlated, the model based on  $\ln(V_{S30})$  will explain some, but not all, of the dependence of the site term on  $\ln(\text{mHVSR}^*)$ . As a result, the correlation of  $\ln(\text{mHVSR}^*)$

with the relative site term is smaller than seen in Figure 12 for the total site term in which the  $V_{S30}$  scaling is not included.

The  $R^2$  values for the correlation of  $\delta S2S$  with  $\ln(Z_{1.0}^*)$ ,  $f_0$ ,  $\ln(\text{mHVSR}(T))$ , and  $\ln(\text{mHVSR}^*(T))$  are shown in Figure 14. For the relative site terms, the normalized amplitude has larger correlations than for the  $f_0$  at all periods and has larger correlations than the unnormalized amplitude for  $T \leq 2.5$  s. For periods of 3–4 s, the unnormalized mHVSR has slightly larger correlations. If the  $V_{S30}$  value is known, then the  $R^2$  values for  $\ln(\text{mHVSR}^*)$  are much larger than for  $\ln(Z_{1.0}^*)$ , indicating that  $\ln(\text{mHVSR}^*)$  contains more information that is different from that given by the  $V_{S30}$  than  $\ln(Z_{1.0}^*)$  for this set of California sites.

### EMPIRICAL MODEL OF SITE AMPLIFICATION USING mHVSR

In this section, we derive two empirical models for the site terms using the normalized  $\ln(\text{mHVSR}^*)$  parameter: one model for the total site terms and one model for the site term relative to the scaling in the

GMM. The model for the total site term can be used if a  $V_{S30}$  measurement is not available, but a mHVSR is available. If the  $V_{S30}$  is available, then the model for the relative site term should be used, because  $V_{S30}$  and mHVSR together provide a better constraint on the site term than either parameter by themselves. As shown subsequently, the general functional form for the site amplification used in our model is consistent with previous models developed by Senna *et al.* (2008), Ghofrani *et al.* (2013), and Kawase, Nagashimo, Nakano, and Mori (2018), but we allow additional flexibility in the scaling of the site amplification with the mHVSR.

Senna *et al.* (2008) proposed an empirical site amplification model based on HVSR from microtremors. Their site amplification is relative to a reference spectrum,  $SA_b(T)$ , and the model is given by:

$$\frac{SA_s(T)}{SA_b(T)} = \frac{m\text{HVSR}(T)}{\alpha_k \beta_m(T)}, \quad (7)$$

in which  $\alpha_k$  is a factor based on a geologic or topographic unit group and  $\beta_m(T)$  is a period-dependent factor from a classification based on the HVSR shape. The period-dependent amplification factor,  $\text{AF}(T)$ , can be written as:

$$\ln(\text{AF}(T)) = \ln(m\text{HVSR}(T)) - \ln(\alpha_k \beta_m(T)). \quad (8)$$

Ghofrani *et al.* (2013) analyzed the site effects induced by the 2011  $M_w$  9.0 Tohoku, Japan, earthquake. They developed a model which captures the linear site amplification based on the  $V_{S30}$ ,  $f_0$ , and the earthquake HVSR amplitude. Their model for the  $\text{AF}(T)$  can be written as:

$$\begin{aligned} \ln(\text{AF}(T)) = & a_1(T) + \ln(e\text{HVSR}(T)) \\ & + a_2(T) \ln\left(\frac{V_{S30}}{760}\right) + a_3(T) \ln(f_0). \end{aligned} \quad (9)$$

They estimated the model coefficients using the observed data from the Tohoku earthquake.

Kawase, Nagashima, Nakano, and Mori (2018) proposed the double-empirical approach in which two sets of empirical factors are developed for computing the site amplification based on mHVSR. The first set of empirical factors models the ratio of the earthquake HVSR to the microtremors HVSR. The second set of empirical factors models the ratio of the vertical component at the surface to the horizontal component for the rock at depth. These two empirical models are combined with the measured mHVSR to compute the total site amplification for the horizontal component. The amplification factor for the double-empirical model can be written as:

$$\left(\frac{H_{\text{surf}}}{H_{\text{rock}}}\right)_{\text{SC}} = \left(\frac{e\text{HVSR}}{m\text{HVSR}}(T)\right)_{\text{SC}} \left(\frac{V_{\text{surf}}}{H_{\text{rock}}}(T)\right)_{\text{SC}} m\text{HVSR}(T), \quad (10)$$

in which SC is the index for the site class,  $\left(\frac{e\text{HVSR}}{m\text{HVSR}}(T)\right)$  is an empirical period-dependent factor which accounts for the difference between the amplitudes of the HVSR from earthquakes and microtremors measured at the ground surface, and  $\left(\frac{V_{\text{surf}}}{H_{\text{rock}}}(T)\right)$  is an empirical model for the period-dependent ratio of the vertical motion at the surface to the horizontal motion on rock at depth. The product of the first two terms is an estimate of the site-specific eHVSR at the ground surface. Multiplying by the last term converts the eHVSR to a horizontal site amplification from rock at depth to the surface. This formulation has the advantage that it keeps the problem separated into the two main topics that have been studied: (1) the difference between HVSR from earthquakes and microtermor and (2) the estimation of horizontal site amplification from the earthquake HVSR. Kawase, Nagashima, Nakano, and Mori (2018) developed the two empirical models for the period-dependent ratios for five different site

classes using the Japanese strong-motion datasets with both surface and downhole recordings. The sites were classified based on the predominant period of the mHVSR. The model can be written in terms of the logarithm of the amplification factor:

$$\begin{aligned} \ln(\text{AF}_{\text{SC}}(T)) = & \ln\left(\frac{e\text{HVSR}}{m\text{HVSR}}(T)\right)_{\text{SC}} + \ln\left(\frac{V_{\text{surf}}}{H_{\text{rock}}}(T)\right)_{\text{SC}} \\ & + \ln(m\text{HVSR}(T)). \end{aligned} \quad (11)$$

Combining the two empirical ratios into a single period-dependent term,  $C_{\text{SC}}(T)$ , leads to the following form of the model:

$$\ln(\text{AF}_{\text{SC}}(T)) = C_{\text{SC}}(T) + \ln(m\text{HVSR}(T)). \quad (12)$$

The Senna *et al.* (2008), Ghofrani *et al.* (2013), and Kawase, Nagashima, Nakano, and Mori (2018) models have the following general form:

$$\ln(\text{AF}(T)) = C_1(T, \text{site}) + 1.0 \ln(\text{HVSR}(T)), \quad (13)$$

in which site can be a site class or a parametric site term such as  $V_{S30}$ . A key feature of these models is that the slope on the  $\ln(\text{HVSR}(T))$  term is constrained to be unity. In our model, we let the slope on the  $\ln(\text{HVSR}(T))$  term to be a free parameter. We use a model with the following functional form:

$$\overline{\delta S2S}(T) = C_1(T) + C_2(T) \ln(m\text{HVSR}^*(T)), \quad (14)$$

in which  $C_1(T)$  and  $C_2(T)$  are period-dependent coefficients that are independent of the class for sites with  $V_{S30} < 1000$  m/s.

As will be shown in the mHVSR Site Term Model section, we find that the slope on the  $\ln(m\text{HVSR})$  term is smaller than unity for the California dataset. This supports allowing the slope to be a free parameter in the regression and not constraining it to unity. This formulation is also consistent with the linear trend observed on Figure 11. As we discussed in the Site terms section, we use a normalized HVSR,  $(m\text{HVSR}^*(T))$ .

Because the  $V_{S30}$  is correlated with the  $m\text{HVSR}^*(T)$ , the empirical relation between the  $\ln(m\text{HVSR}^*(T))$  and  $\delta S2S'$  (site terms without the  $V_{S30}$  scaling) will be different than the relation between  $\ln(m\text{HVSR}^*(T))$  and  $\delta S2S$ . To indicate different scaling for  $\delta S2S$  and  $\delta S2S'$ , coefficients  $C_3$  and  $C_4$  are used for the model for the total site amplification:

$$\begin{aligned} \overline{\delta S2S}(T) = & C_3(T) \\ & + C_4(T) \ln(\text{HVSR}^*(T)). \end{aligned} \quad (15)$$

### mHVSR SITE TERM MODEL FOR THE ASK14 GMM

Empirical models for HVSR scaling of the site terms are developed for the case without  $V_{S30}$  measurements ( $\delta S2S'$ ) and for the case with  $V_{S30}$  measurements ( $\delta S2S$ ). Ordinary least-squares is used to estimate the coefficients. The estimated coefficients and their standard errors are listed in Tables 1 and 2 for these two cases.

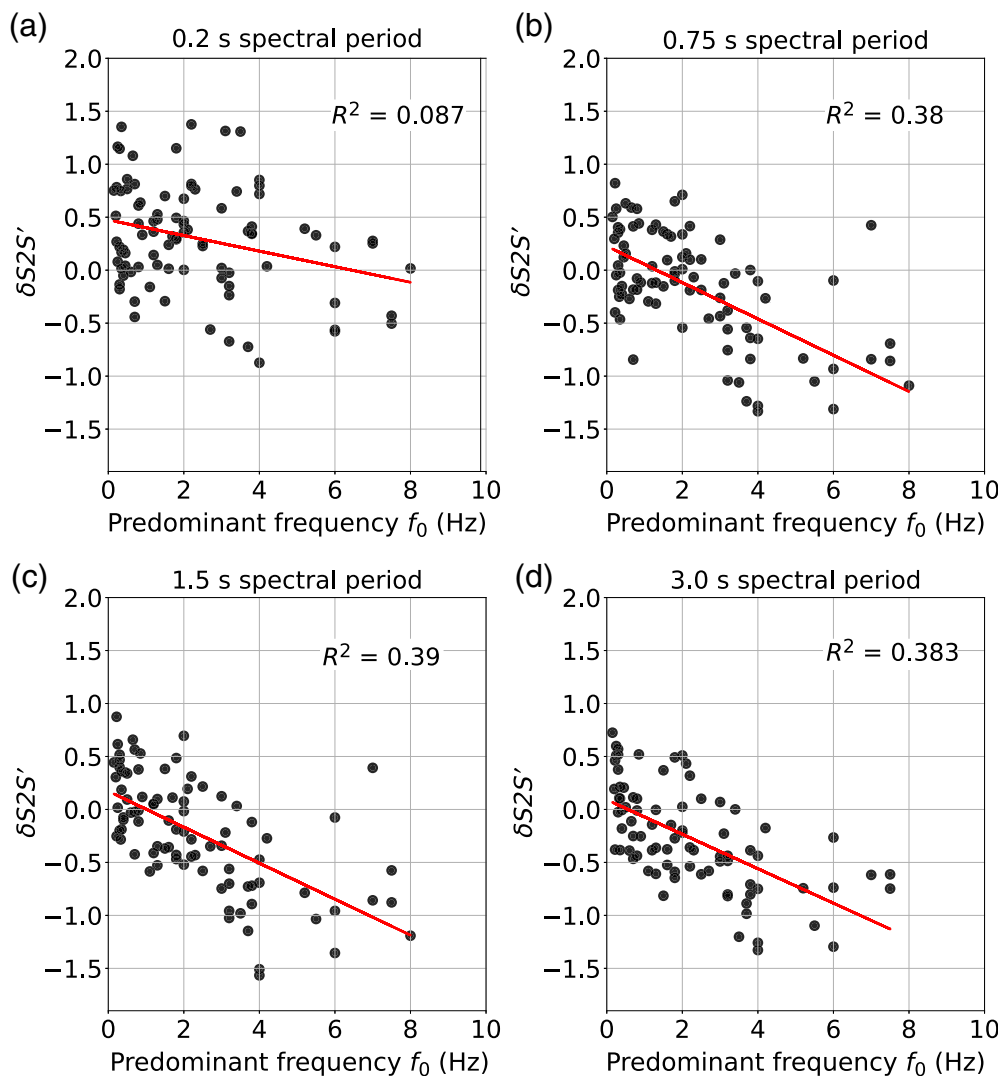


**Figure 10.** Scatter plot showing the correlation between the site terms without the ASK14  $V_{S30}$  scaling,  $\delta S'_{S2S}$ , and the predominant frequency,  $f_0$ , for four spectral periods: (a) 0.2 s spectral period, (b) 0.75 s spectral period, (c) 1.5 s spectral period, and (d) 3.0 s spectral period. This subset only includes 90 stations that had clear predominant frequencies, according to the [SESAME Project \(2004\)](#) criteria. The color version of this figure is available only in the electronic edition.

The  $R^2$  values for the two cases are compared in Figure 15. For the case without measured  $V_{S30}$ , the  $R^2$  values for  $\ln(\text{mHVS}R^*)$  range from zero at short periods to 0.54 at long periods. The residuals are shown as a function of  $V_{S30}$  in Figure 16. The trend in the residuals with  $V_{S30}$  is expected because the  $\text{mHVS}R^*$  is only partially correlated with  $V_{S30}$ , so the model based on  $\ln(\text{mHVS}R^*)$  will not explain all of the  $\ln(V_{S30})$  scaling. That is, some of the negative slope shown in Figure 8 can be explained by  $\text{mHVS}R^*$ , but not all of it.

For the case with measured  $V_{S30}$ , the  $R^2$  values for  $\ln(\text{mHVS}R^*)$  range from zero at short periods to 0.25 at long periods as shown in Figure 15. These  $R^2$  values indicate the additional improvement in the estimate of the site term that results by having  $\text{mHVS}R$  measurements at a site in addition to the

$V_{S30}$ . The  $R^2$  values are smaller than for the case without  $V_{S30}$  scaling because some of the  $\text{mHVS}R^*$  scaling is accommodated by the  $V_{S30}$  scaling. The residuals as a function of  $\ln(\text{mHVS}R^*)$  and  $\ln(V_{S30})$  are shown in Figures 17 and 18. There is no trend in residuals with either  $\ln(\text{mHVS}R^*)$  or  $V_{S30}$  after including the  $\text{mHVS}R$  data, indicating that the coefficients are applicable to all sites represented in the selected dataset.

An  $R^2$  value of 0.2 may be considered weak correlation to researchers in other fields, but it is a significant correlation for GMMs. Terms with  $R^2$  values less than 0.2 are commonly included in GMMs. For example, in Figure 14, the  $R^2$  values for  $Z_{1.0}^*$  are less than 0.2 at all periods if the  $V_{S30}$  is known, but basin effects are considered important, and they are included in the NGA-W2 GMMs. Similarly, the  $R^2$  for the style-of-faulting factors in the ASK14 GMM is less than 0.15, but the style-of-faulting class is included as a predictive parameter in GMMs. Even though a parameter may have an  $R^2$  value of only 0.2, that does not mean that it is not important to include in the GMM.

For example, by including site-specific measurements of  $\text{mHVS}R$  in addition to  $V_{S30}$ , the median ground motions at long periods can vary by up to a factor of 1.6 relative to the median ground motion estimated without an  $\text{mHVS}R$  measurement, even though the  $R^2$  values are only about 0.2 at long periods. This shows that including parameters with  $R^2$  as low as 0.2 can still have a significant effect on the resulting ground motion and hazard analysis due mainly to the change in the median, not the reduction in the aleatory standard deviation.

The  $C_2$  and  $C_4$  coefficients are smoothed as a function of period for inclusion into the GMMs. The smoothing is shown in Figure 19. For periods less than  $T = 0.1$  s, the  $C_2$  term becomes negative, indicating that a larger  $\text{HVS}R$  ratio at short periods leads to smaller response spectral values at these short

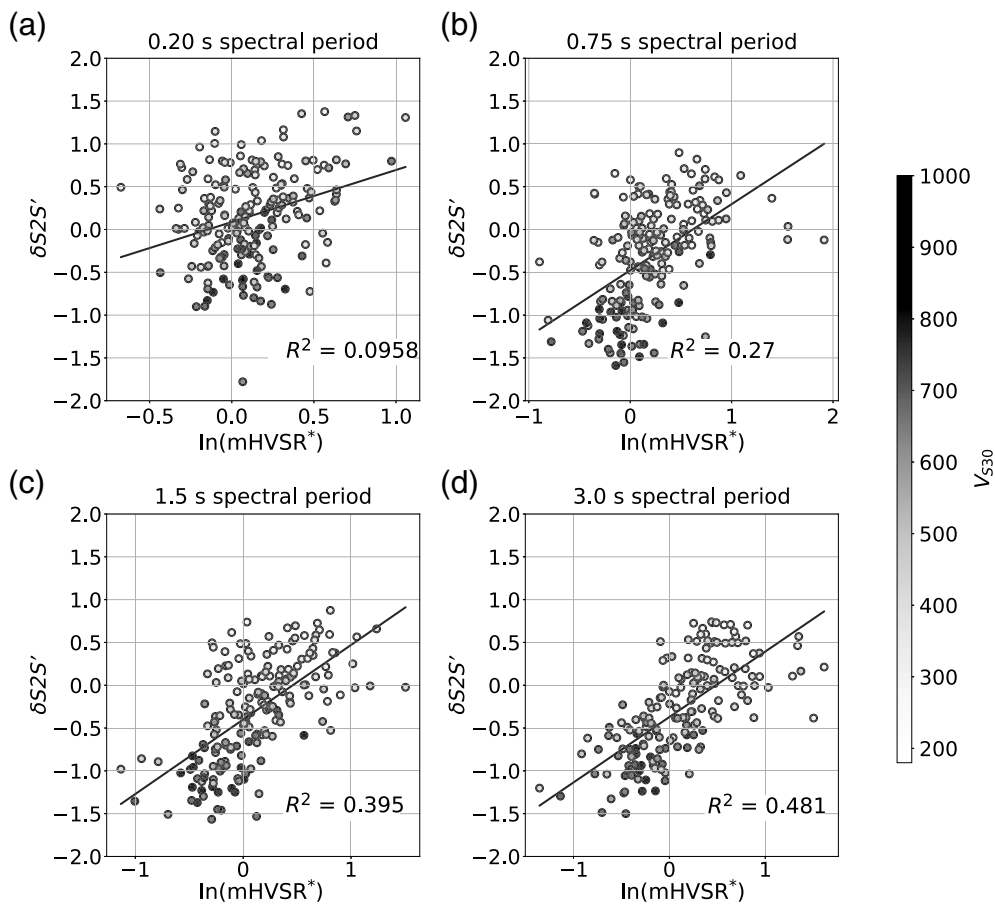


**Figure 11.** Scatter plot between the site terms without the ASK14  $V_{S30}$  scaling,  $\delta S_{2S}'$ , and the normalized mHVSr\* from microtremor for four spectral periods: (a) 0.2 s spectral period, (b) 0.75 s spectral period, (c) 1.5 s spectral period, and (d) 3.0 s spectral period. The colors of the symbols show the  $V_{S30}$  for each site.

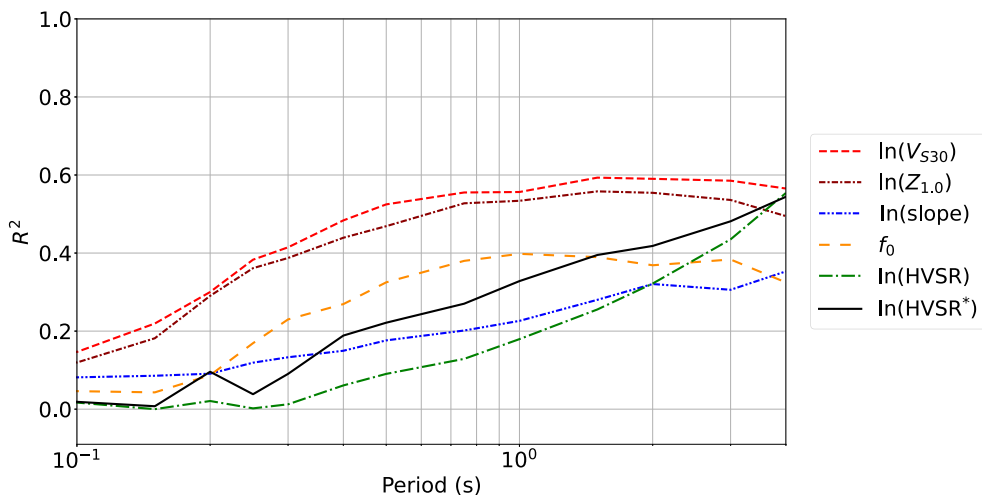


**Figure 12.** Period dependence of the  $R^2$  values for the five site parameters for the case without the  $V_{S30}$  scaling and the depth basin factor from the ASK14 ground-motion model (GMM). The color version of this figure is available only in the electronic edition.

periods. The negative value of  $C_2$  may be a result of the difference between FAS used for the HVSR and the PSA used for the GMM: at short periods, the PSA is affected by a range of periods and does not represent the amplitude of the motion at the natural period of the oscillator (Bora *et al.*, 2016). Without a good physical basis for the negative  $C_2$  values at short periods for PSA, we set  $C_2 = 0$  for periods less than or equal to 0.15 s. The smoothed  $C_4$  term for the  $\delta S_{2S}'$  values without measured  $V_{S30}$  is also shown in Figure 19. The  $C_4$  values increase with period, peaking at  $T = 1.0$ – $2.0$  s, compared to peaking at  $T = 0.3$ – $0.75$  s for the case with measured  $V_{S30}$ . This reduction in the period of the peak effect is due to the  $V_{S30}$  scaling being strongest in the range 1.0–1.5 s. The smoothed model coefficients are listed in Table 3.

The  $R^2$  values are also smoothed as function of period for use in seismic hazard applications (Fig. 20) to quantify the epistemic uncertainty in the site terms. These  $R^2$  values are computed from data mainly in the range  $M$  3.5–5. Therefore, they are directly applicable to compute the reduction in  $\phi_{S2S}$  for  $M$  5 due to the additional information from the mHVSr data. A correction for application to larger magnitudes is described in the example in the following section.

### EXAMPLE PROBABILISTIC HAZARD APPLICATION

For probabilistic seismic hazard applications (PSHA), the mHVSr scaling can be directly included in the GMM used in the PSHA calculation, resulting

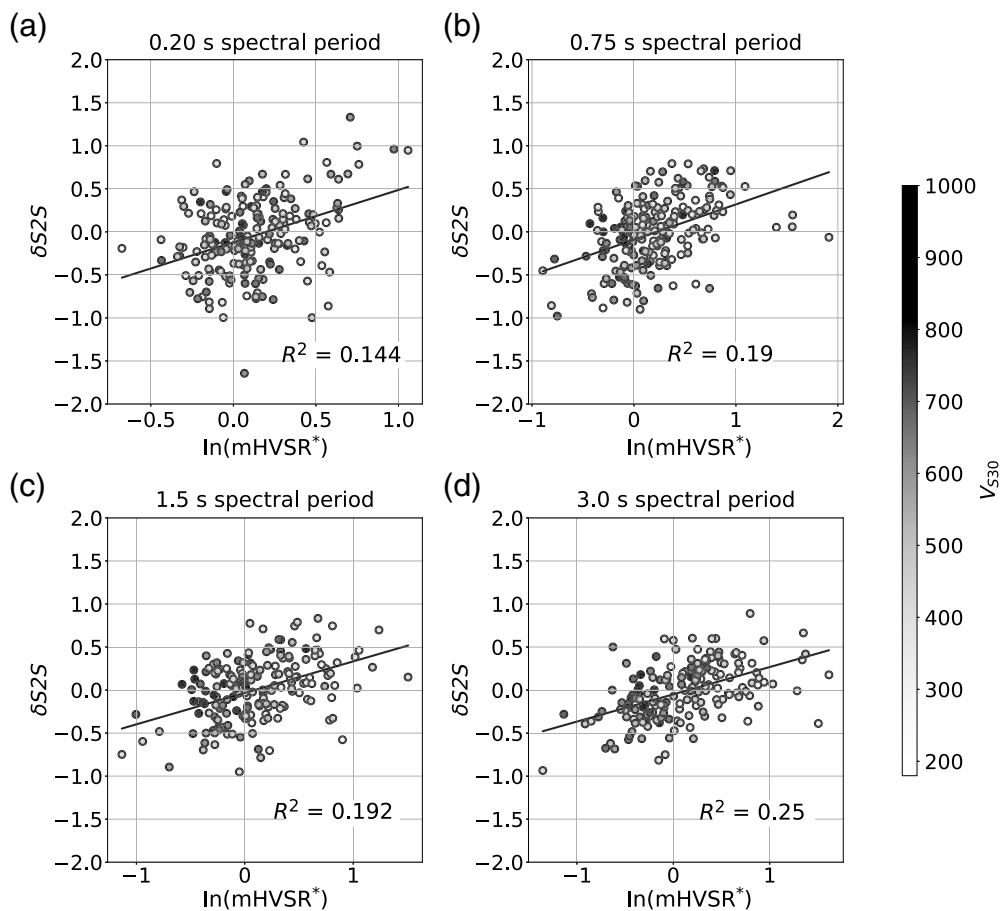


**Figure 13.** Correlation of the site terms with the ASK14  $V_{S30}$  scaling,  $\delta S_{2S}$ , and the normalized  $\ln(\text{mHVSr}^*)$  from microtremor for four spectral periods: (a) 0.2 s spectral period, (b) 0.75 s spectral period, (c) 1.5 s spectral period, and (d) 3.0 s spectral period. The colormap represents the  $V_{S30}$ .

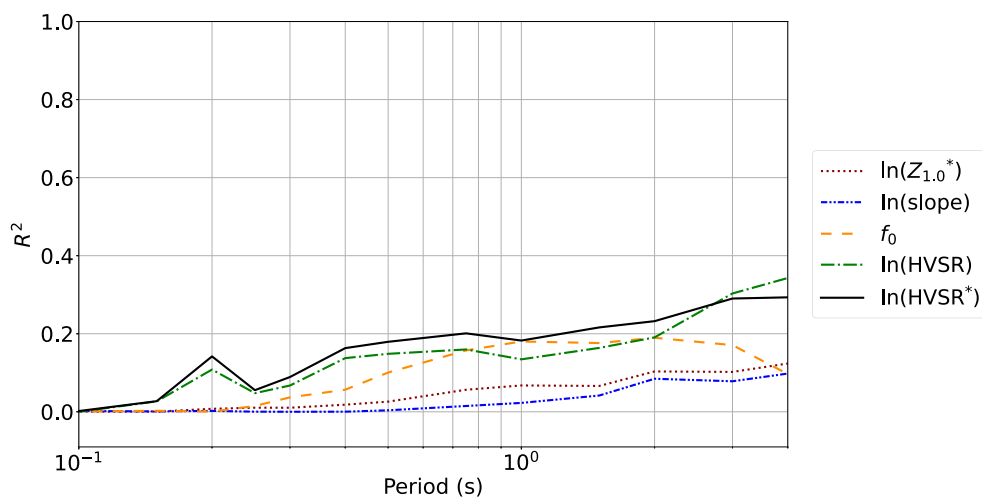


**Figure 14.**  $R^2$  values for the site parameters for the case with the ASK14  $V_{S30}$  scaling (equation 14). The color version of this figure is available only in the electronic edition.

in a change in the median and a reduction of the standard deviation. An alternative is to use the mHVSr data to estimate the site-specific term in a partially nonergodic seismic hazard approach. This has the advantage that it allows the hazard to be computed using current GMMs with the mHVSr scaling to estimate the site-specific site terms. It also quantifies the benefits of collecting mHVSr data at project sites which can help to convince project engineers of the value of collecting mHVSr measurements at their site. The partially nonergodic approach is summarized subsequently.

### Partially nonergodic GMM

In a partially nonergodic GMM, each site has its own average site response that will differ from the average site response for a given  $V_{S30}$  and  $Z_{1.0}$ . The difference between the median linear site-specific amplification and the median linear amplification given by the GMM for the  $V_{S30}$  and  $Z_{1.0}$  of the site is denoted  $\delta S_{2S_s}$ . In the ergodic approach,  $\delta S_{2S_s}$  is assumed to be a random variable that could occur at any site during a future earthquake (i.e., it is treated as part of the aleatory variability). In the partially nonergodic GMM approach,  $\delta S_{2S_s}$  applies to a specific site rather than to all sites.

The standard deviation of  $\delta S_{2S_s}$ , denoted  $\phi_{S_{2S_s}}$ , indicates how much of the average linear site amplification is not captured by the simple  $V_{S30}$  and basin depth ( $Z_{1.0}$  or  $Z_{2.5}$ ) scaling in the GMM. It represents the epistemic uncertainty in the site-specific site amplification if there are no additional

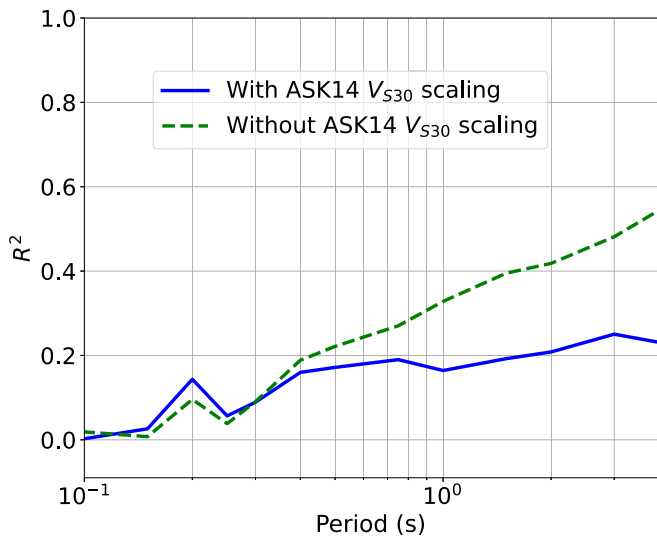


**Figure 15.**  $R^2$  values for the normalized mHVS $r^*$ , for the case without ASK14  $V_{S30}$  scaling ( $\delta S2S'$ ) and the case with the ASK  $V_{S30}$  scaling ( $\delta S2S$ ). The color version of this figure is available only in the electronic edition.

**TABLE 1**  
**Regression Coefficients for  $\delta S2S$**

Period (s)	$\phi_{SS}$	$R_1^2$	$C_1$	$C_2$	SE $C_2$	Standard Deviation
0.050	0.542	0.062	-0.113	-0.286	0.073	0.416
0.100	0.557	0.003	-0.072	-0.124	0.160	0.475
0.150	0.564	0.026	-0.067	0.331	0.133	0.464
0.200	0.559	0.144	-0.128	0.658	0.106	0.421
0.250	0.556	0.057	-0.103	0.363	0.098	0.417
0.300	0.550	0.089	-0.114	0.433	0.092	0.405
0.400	0.521	0.160	-0.131	0.506	0.075	0.375
0.500	0.514	0.172	-0.116	0.440	0.063	0.362
0.750	0.479	0.190	-0.098	0.455	0.061	0.358
1.000	0.461	0.164	-0.069	0.403	0.059	0.353
1.500	0.447	0.192	-0.036	0.397	0.055	0.329
2.000	0.430	0.208	-0.036	0.390	0.051	0.318
3.000	0.418	0.250	-0.054	0.375	0.041	0.289
4.000	0.389	0.231	-0.071	0.344	0.041	0.275

These coefficients are for sites with measured  $V_{S30}$ . SE, standard error.

data to constrain the site-specific amplification. That is, without site-specific data, the amplification at the site could be  $\delta S2S'$  from any of the sites in the dataset used in the regression.

For this form of a partially nonergodic GMM, the aleatory variability is given by the single-station sigma:

$$\sigma_{ss} = \sqrt{\tau^2 + \phi_{SS}^2} = \sqrt{\tau^2 + (\phi^2 - \phi_{S2S}^2)}, \quad (16)$$

in which  $\phi_{S2S}$  is the standard deviation of the site terms. Previous studies have developed estimates of  $\sigma_{ss}$  for use in partially nonergodic PSHA. A comparison of the period

**TABLE 2**  
**Regression Coefficients for  $\delta S2S'$**

Period (s)	$\phi_{SS}$	$R_2^2$	$C_3$	$C_4$	SE $C_4$	Standard Deviation
0.050	0.542	0.078	0.207	-0.364	0.083	0.470
0.100	0.557	0.019	0.276	-0.362	0.174	0.512
0.150	0.564	0.008	0.294	0.200	0.154	0.533
0.200	0.559	0.096	0.083	0.643	0.133	0.525
0.250	0.556	0.038	-0.035	0.382	0.130	0.548
0.300	0.550	0.090	-0.193	0.577	0.125	0.543
0.400	0.521	0.189	-0.409	0.769	0.108	0.530
0.500	0.514	0.222	-0.463	0.730	0.093	0.526
0.750	0.479	0.270	-0.482	0.811	0.091	0.525
1.000	0.461	0.328	-0.462	0.863	0.085	0.491
1.500	0.447	0.395	-0.404	0.899	0.079	0.461
2.000	0.430	0.418	-0.368	0.875	0.073	0.446
3.000	0.418	0.481	-0.374	0.817	0.060	0.398
4.000	0.390	0.544	-0.396	0.846	0.056	0.356

These coefficients are for sites without measured  $V_{S30}$ .

**TABLE 3**  
**Smoothed Model Coefficients**

Period (s)	With $V_{S30}$ Measurement			Without $V_{S30}$ Measurement		
	$C_1$	$C_2$	$R^2$	$C_3$	$C_4$	$R^2$
0.05	0	0	0	0	0.000	0
0.1	0	0	0	0	0.000	0
0.15	-0.069	0.414	0	0.292	0.266	0
0.2	-0.103	0.449	0.043	0.108	0.432	0.050
0.25	-0.121	0.465	0.076	-0.062	0.538	0.089
0.3	-0.121	0.472	0.104	-0.199	0.610	0.120
0.4	-0.125	0.473	0.147	-0.395	0.701	0.170
0.5	-0.123	0.466	0.180	-0.470	0.756	0.209
0.75	-0.098	0.444	0.188	-0.487	0.824	0.280
1	-0.075	0.423	0.193	-0.462	0.853	0.330
1.5	-0.036	0.393	0.201	-0.401	0.878	0.400
2	-0.035	0.375	0.207	-0.369	0.889	0.437
3	-0.054	0.360	0.214	-0.379	0.830	0.488
4	-0.070	0.360	0.220	-0.392	0.830	0.525

dependence of the ergodic standard deviation,  $\sigma$ , from the ASK14 GMM and the partially nonergodic standard deviation,  $\sigma_{SS}$ , from the southwestern U.S. (SWUS) GMM (Geopentech, 2015) is shown in Figure 21. The  $\phi_{S2S}$  values shown in Figure 21 are back calculated from the ASK14  $\sigma$  and the SWUS  $\sigma_{SS}$ :

$$\phi_{S2S} = \sqrt{\sigma^2 - \sigma_{SS}^2}. \quad (17)$$

At short periods, there is a strong magnitude dependence of  $\sigma$  and a weak magnitude dependence of  $\sigma_{SS}$ , so the computed  $\phi_{S2S}$  is magnitude dependent at short periods (Fig. 22). Part of this magnitude dependence may reflect nonlinear site effects, but

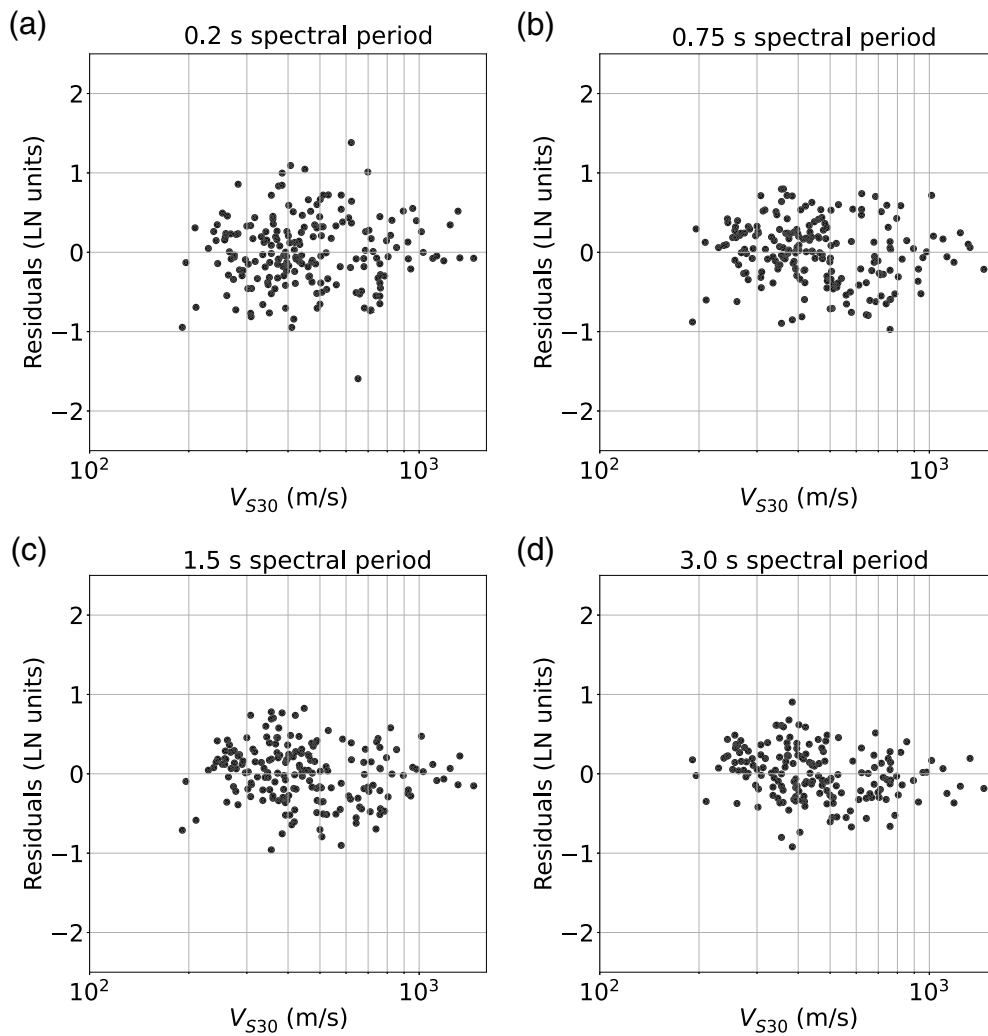


**Figure 16.** Pseudospectral acceleration (PSA) residuals for the case without ASK14  $V_{S30}$  scaling as a function of  $V_{S30}$  for four periods: (a)  $T = 0.2$  s, (b)  $T = 0.75$ , (c)  $T = 1.5$  s, and (d)  $T = 3$  s.

most of the ground-motion data used to develop the GMM and  $\sigma$  models are in the linear range. Intuitively, the linear site terms should not be magnitude dependent, so  $\phi_{S2S}$  should not be magnitude dependent; however, the amplification for response spectral values depends on the spectral shape (i.e., the calculation of the response spectral values is a nonlinear operation even for small strains). The small-magnitude events have greater high-frequency content compared to large-magnitude events which leads to greater variability of the high-frequency response spectral amplification factors for the small-magnitude events.

To implement the partially nonergodic approach in a PSHA, both the best estimate and the epistemic uncertainty of site-specific  $\delta S2S_s$  term are needed.

For seismic hazard applications using partially nonergodic GMMs, the epistemic uncertainty in  $\delta S2S$  needs to be included in the logic tree to justify the use of the reduced aleatory variability ( $\sigma_{ss}$  versus  $\sigma$ ). If a measured  $V_{S30}$  for the site is available, then the epistemic uncertainty of  $\delta S2S$ , denoted  $\phi_{S2S-mHV1}(T)$ ,

depends on the value of  $R^2(T)$  and  $\phi_{S2S}(T, M)$ :

$$\begin{aligned} \phi_{S2S-mHV1}(T, M) \\ = \phi_{S2S}(T, M) \sqrt{1 - R_1^2(T)}. \end{aligned} \quad (18)$$

If a measured  $V_{S30}$  is not available, then  $\phi_{S2S}$  is increased to reflect the standard deviation of the site term from the GMM for the dataset used to develop the mHVS $R^*$  factors. Here, we use the standard deviation of the site terms ( $f_5 + f_{10}$ ),  $\phi_{V_{S30}}$ , computed using the ASK14 GMM for the 196 stations in the dataset.  $\phi_{V_{S30}}$  is combined with the empirical model for  $\phi_{S2S}(M, T)$ . The resulting epistemic uncertainty in the non-ergodic site term for the case without measured  $V_{S30}$ , denoted  $\phi_{S2S-mHV2}(T)$ , is given by:

$$\begin{aligned} \phi_{S2S-mHV2}(T, M) \\ = \sqrt{\phi_{S2S}^2(T, M) + \phi_{V_{S30}}^2} \\ \sqrt{1 - R_2^2(T)}. \end{aligned} \quad (19)$$

For seismic hazard applications, we need the epistemic uncertainty in the nonergodic

site term for larger magnitudes and not just for the small magnitudes ( $M$  3–5) that dominate the dataset.  $\phi_{S2S}$  has a magnitude dependence as shown in Figure 22. We assume that  $R^2$  for large magnitude events is the same as for small magnitude events. For the case with measured  $V_{S30}$ , we use equation (18) to compute the epistemic uncertainty using the empirical magnitude-dependent  $\phi_{S2S}$  shown in Figure 22. The resulting epistemic uncertainties for the nonergodic site term are listed in Table 4. Similarly, for the case without measured  $V_{S30}$ , we use equation (19). The epistemic uncertainties for this case are larger than for the case with measured  $V_{S30}$  as shown in Table 4.

In the partially nonergodic approach, the ergodic GMM median is shifted by  $\delta S2S$  and the aleatory variability is given by  $\sigma_{ss}$ . A logic tree is used to sample the epistemic uncertainty range of  $\delta S2S$ . If there is measured  $V_{S30}$  but no site-specific measurements of mHVS $R$  available, then the best estimate  $\delta S2S$  is zero and the epistemic uncertainty of  $\delta S2S$  has a standard deviation of  $\phi_{S2S}$ . If there are site-specific measurements of the

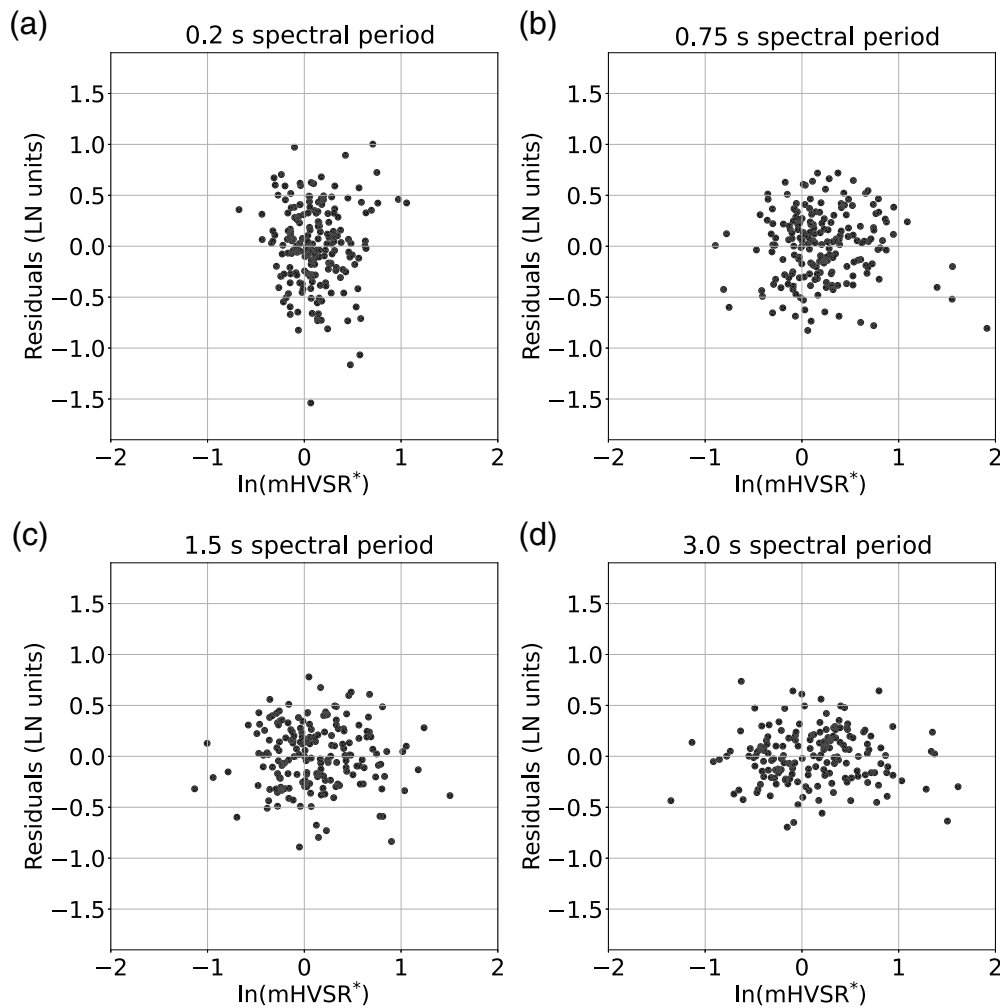


**Figure 17.** PSA residuals including the  $V_{S30}$  scaling from the ASK14 GMM as a function of HVSR\* for four periods: (a)  $T = 0.2$  s, (b)  $T = 0.75$  s, (c)  $T = 1.5$  s, and (d)  $T = 3$  s.

mHVSR\* available, then the epistemic uncertainty in  $\delta S2S$  is reduced and is given by a normal distribution with mean  $\overline{\delta S2S}$  given by equation (14) and standard deviation  $\phi_{S2S-mHV}$  given by equations (18) or (19) depending on the availability of a  $V_{S30}$  measurement:

$$\delta S2S \sim \mathcal{N}(\overline{\delta S2S}, \phi_{S2S-mHV}). \quad (20)$$

With the additional information from the measurements of mHVSR at the site, the site-specific epistemic uncertainty is reduced from the traditional epistemic uncertainty of the site term,  $\phi_{S2S}$  from the GMM, to the mHVSR-based epistemic uncertainty,  $\phi_{S2S-mHV}$ .

As an example application, the seismic hazard is computed for a site located in Oakland California, 6 km from the Hayward fault. The seismic source characterization uses the time-dependent earthquake probabilities from the Working Group on Earthquake Probabilities for the San Francisco Bay area (Working Group on California Earthquake Probabilities

[WGEP], 2003). The site condition is set at  $V_{S30} = 400$  m/s with default  $Z_{1.0}$  and  $Z_{2.5}$  values. The ergodic mean hazard for  $T = 2$  s, computed using the ASK14 GMM, is shown in Figure 23. Using the ergodic approach, the differences in the site terms,  $\delta S2S$ , are treated as part of the aleatory standard deviation.

We first use the partially nonergodic approach for the case without mHVSR data at the site. In this case, the aleatory variability is given by  $\sigma_{ss}$  and the epistemic uncertainty in  $\delta S2S$  is given by  $\phi_{S2S}$ . There is no change in the mean hazard, but the uncertainty fractiles will be wide for the partially nonergodic approach because  $\delta S2S$  is treated as a systematic site-specific effect with epistemic uncertainty.

### Hazard results

To demonstrate the effects of including the mHVSR in a PSHA, we use the estimated  $HVSR^*(T)$  from two sites in the ASK14 dataset: the first site has a positive  $\ln(mHVSR^*(T = 2))$  and the second site has a

negative  $\ln(mHVSR^*(T = 2))$ . The  $\ln(mHVSR^*(T))$  values for the full set of periods for these two sites are listed in Table 5. In this example, we apply the two sets of mHVSR factors to the hazard for the Oakland site. The mHVSR\*-based site terms for the full set of periods are listed also in Table 5. The UHS for a return period of 2500 yr computed using the ergodic approach is compared to the UHS using the partially nonergodic approach with the two sets of mHVSR data in Figure 24. At a period of 2 s, the decrease in the amplification for site 1 ( $\delta S2S = -0.24$ ) is similar to the increase in the amplification for site 2 ( $\delta S2S = 0.23$ ), but the effect on the  $T = 2$  s UHS is not symmetric: for site 1, the  $T = 2$  s UHS is decreased by a factor of 1.38; for site 2, the  $T = 2$  s UHS is increased by a factor of 1.23. The reason for the different scale factors is that the partially nonergodic approach uses a smaller aleatory standard deviation of the GMM ( $\sigma_{ss}$ ) than for the ergodic approach, so although the two sites have symmetric positive and negative  $\delta S2S$  terms, they both use the reduced aleatory variability.



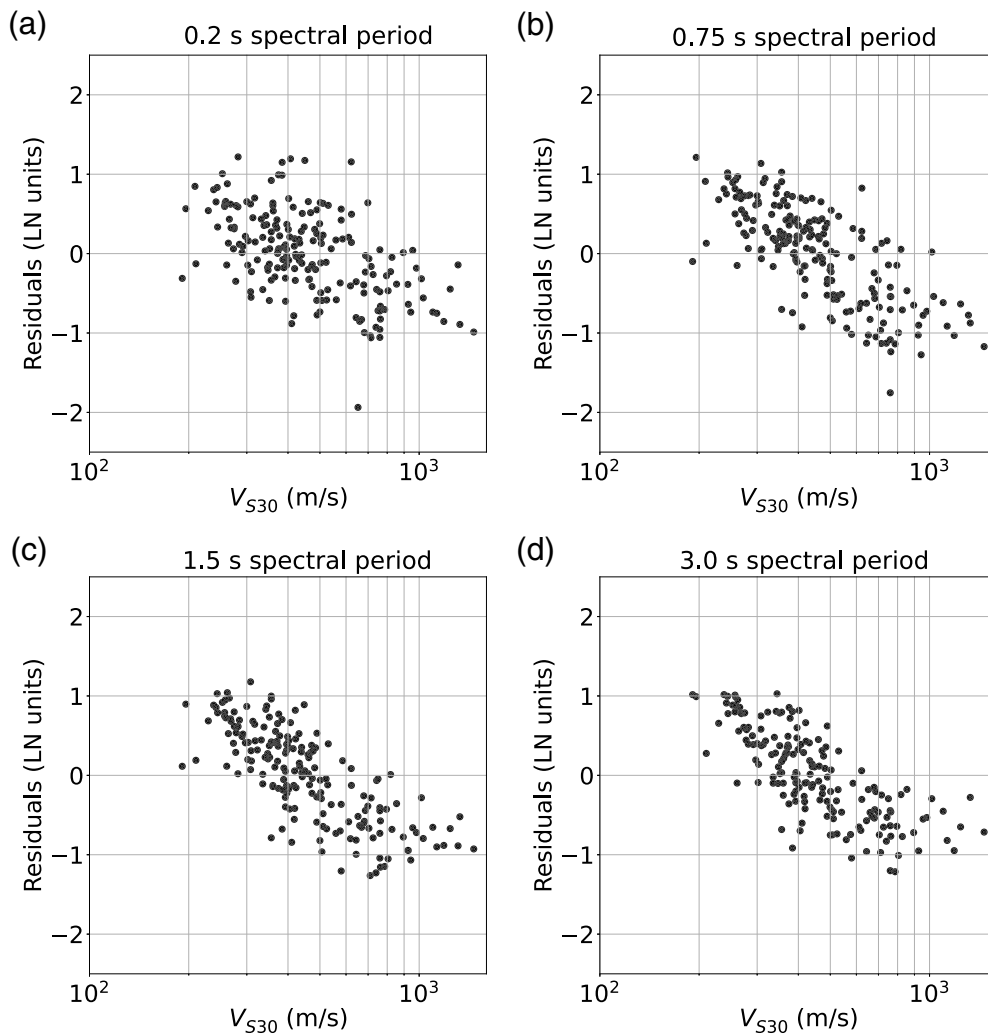


**Figure 18.** PSA residuals including the  $V_{S30}$  scaling from the ASK14 GMM as a function of  $V_{S30}$  for four periods: (a)  $T = 0.2$  s, (b)  $T = 0.75$  s, (c)  $T = 1.5$  s, and (d)  $T = 3$  s.

## CONCLUSIONS

HVSR from microtremors has not been used in site characterization for GMMs for California, but microtremor data measured at the site can provide significant improvements in the accuracy of estimates of the site-specific site amplification at a relatively low cost. Rather than just using mHVSR to determine site categories, the period-dependent normalized amplitude of the mHVSR can be used directly as a site parameter in GMMs and improve the estimation of site-specific site effects at long periods. Alternatively, it can be used to constrain the site term in a partially nonergodic approach. For sites in California with  $V_{S30}$  measurements, the normalized amplitude, mHVSR<sup>\*</sup>, is a better predictor of site amplification than the fundamental site period,  $f_0$ . This may not be the case for other regions that tend to sites conditions that are dominated by velocity profiles with strong impedance contrasts rather than smooth gradients.

The NGA-W2 GMMs capture the site effects through two parameters;  $V_{S30}$  and  $Z_{1.0}$ . If available, the  $V_{S30}$  parameter is a better predictor of the site amplification than mHVSR; however, the combination of the normalized mHVSR and  $V_{S30}$  leads to an improvement in the site amplification prediction at long periods compared to just using  $V_{S30}$ : including the site measurements of mHVSR in addition to  $V_{S30}$  reduces the variance of site-specific site amplification by 20%–25% at long periods. The mHVSR combined with  $V_{S30}$  gives a better estimate of the long-period site amplification than the  $Z_{1.0}$  combined with  $V_{S30}$  as used in current GMMs for California.

The change in the median resulting from the microtremor measurements can lead to significant changes to the hazard compared to the ergodic approach without the microtremor data. The empirical model developed in this study was based on the dataset and residuals from the ASK14 GMM, but these factors are expected to be similar for the other NGA-W2 GMMs for

applications to California due to similar  $V_{S30}$  scaling in the current suite of NGA-W2 GMMs for California sites.

For many projects, it is not practical to measure  $V_{S30}$  at the site due to restrictions on drilling or insufficient space for deploying arrays for surface-wave inversions. In this case, the  $V_{S30}$  is typically estimated using other information such as surface geology or topographic slope. If it is not practical to measure  $V_{S30}$  at a site, measuring mHVSR may be a practical and cost effective alternative for characterizing the site for ground-motion estimation. Although mHVSR measurements are not as good as having a measurement of  $V_{S30}$  for constraining site amplification for California sites, using the mHVSR alone still explains about 40%–50% of the variance of the site-specific amplification at long periods compared to 60% of the variance explained by  $V_{S30}$ . The mHVSR-based proxies have little predictive power for the ground motion at spectral periods less than 0.4 s.

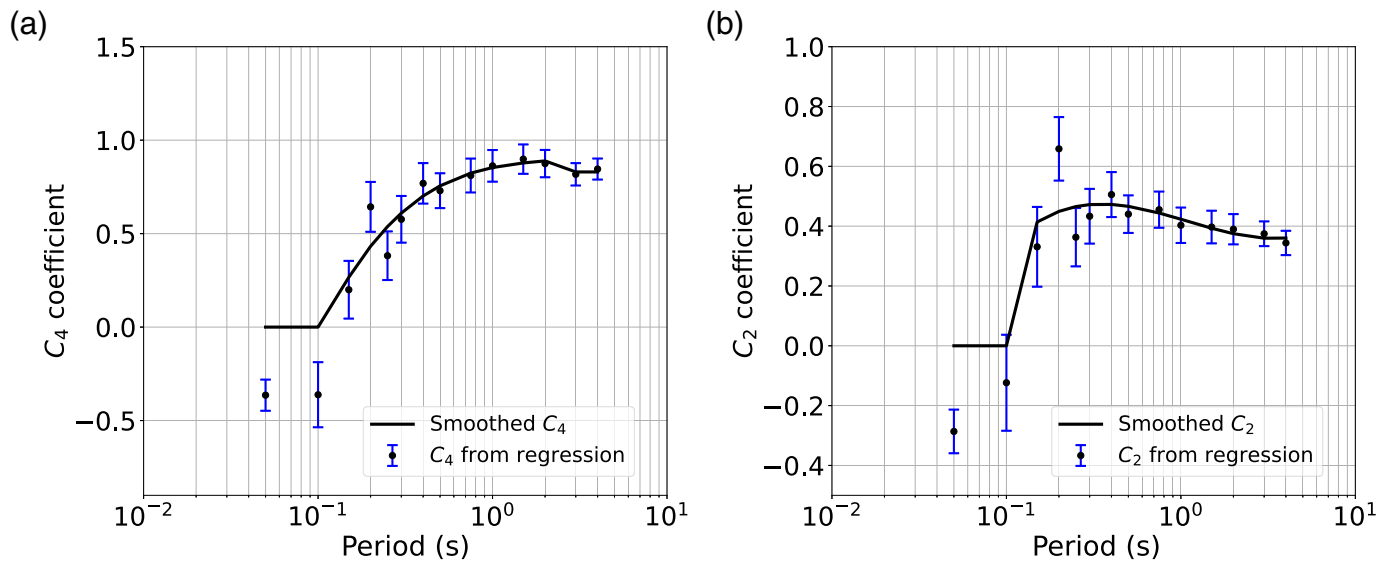


**Figure 19.** Smoothed coefficients for the mHVSr\* slope. (a) Without ASK14  $V_{S30}$  scaling. (b) With ASK14  $V_{S30}$  and  $Z_{1,0}^*$  scaling. The color version of this

figure is available only in the electronic edition.

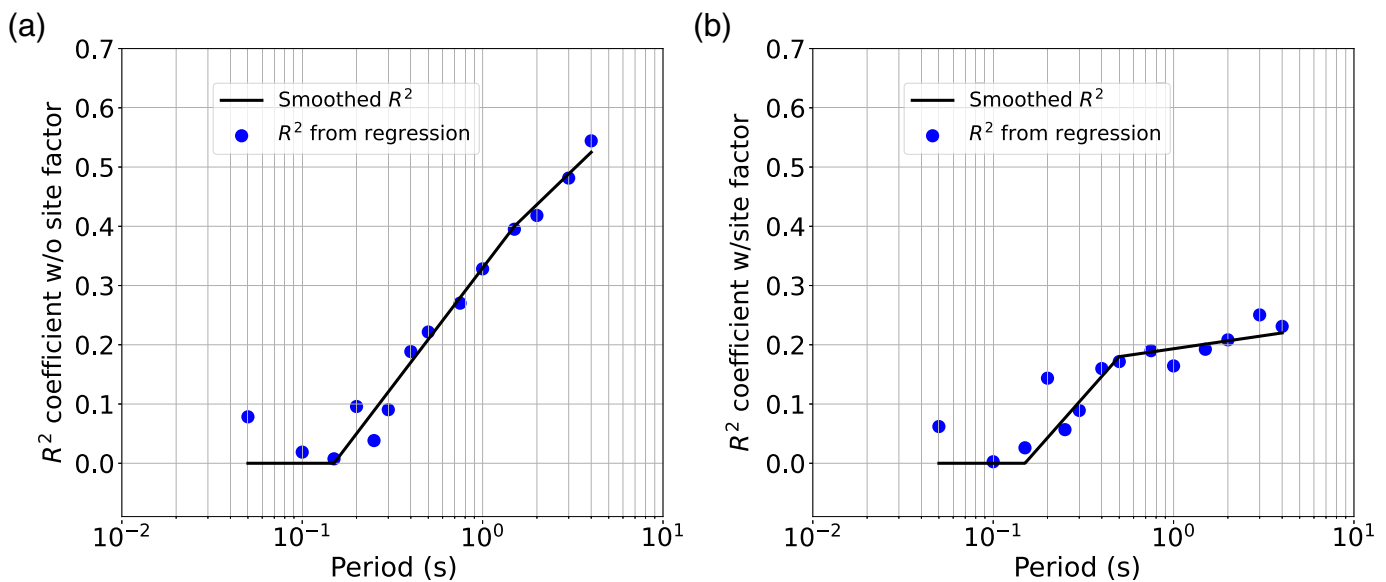


**Figure 20.** Smoothed  $R^2$ . (a) Without ASK14  $V_{S30}$  scaling. (b) With ASK14  $V_{S30}$  and  $Z_{1,0}^*$  scaling. The color version of this figure is available only in the

electronic edition.

There are three main limitations of the current study that should be considered. First, for application of the mHVSr site terms in seismic hazard projects, a key assumption is the mHVSr measured at seismic stations is the same as the mHVSr measured at ground surface at a project site. Because seismic stations are often installed below the ground surface to reduce the background noise, the mHVSr measured from ambient noise recorded by the seismic station may be different from the mHVSr measured at the surface. This assumption

should be tested by measuring mHVSr at the ground surface near seismic stations to quantify the size of the effect.

A second limitation of the current study is that it is based on a subset of only 196 stations that have both ground-motion site terms ( $\delta S2S$ ) from earthquakes in the ASK14 dataset and also continuous recordings for efficient measurement of microtremors. The number of stations can be increased by a campaign to measure microtremor HVSr at sites that do not have continuous recordings but for which GMM residuals

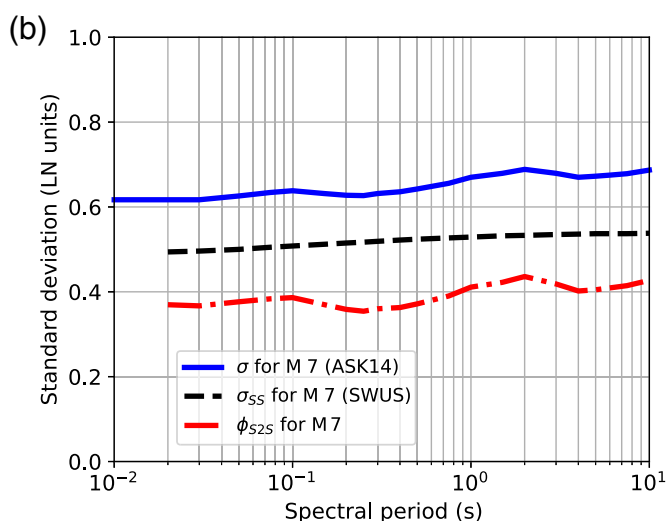
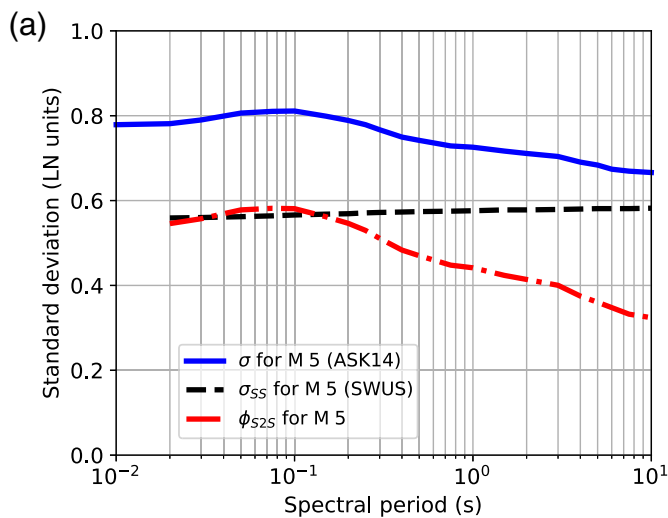


**Figure 21.** Comparison of components of the standard deviation for ergodic and partially nonergodic models. (a) For magnitude 5. (b) For magnitude 7. The color version of this figure is available only in the electronic edition.

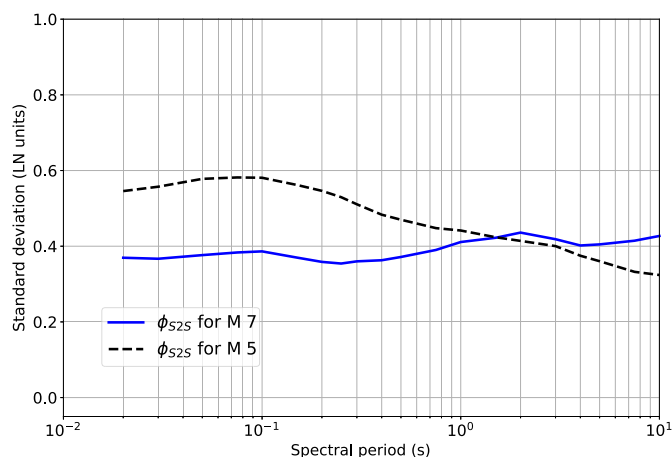


**Figure 22.** Comparison of  $\phi_{525}$  for magnitude 5 and magnitude 7 from the southwestern U.S. (SWUS) model. The color version of this figure is available only in the electronic edition.

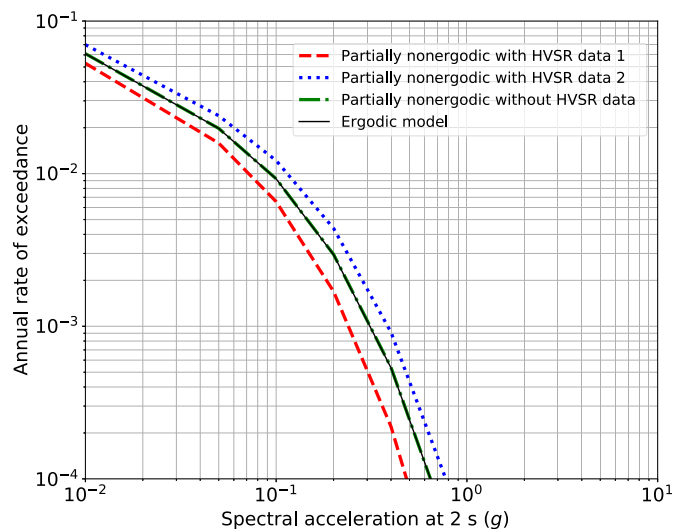


**Figure 23.** Example of the effect on the  $T = 2$  s hazard curves for two estimates of  $mHVSR^*(T)$  from the dataset. The color version of this figure is available only in the electronic edition.

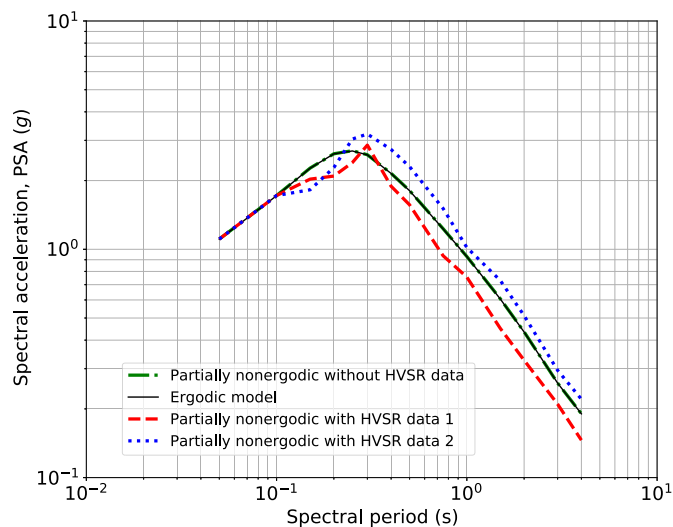


**Figure 24.** Example of the effect on the 2500 yr uniform hazard spectrum (UHS) for two estimates of  $mHVSR^*(T)$  from the dataset. The color version of this figure is available only in the electronic edition.

are available. We recommend taking the measurements at night to reduce the anthropogenic noise effects on the HVSR variability. There is an ongoing initiative to develop a database of HVSR for use in development of future GMMs with HVSR as a predictive parameter (Wang et al., 2021). This database will greatly expand the number of sites for constraining the scaling of site amplification with both HVSR data and earthquake recordings.

A third limitation is the applicability of  $mHVSR$  to hard-rock sites. The dataset used in this study includes only 18 sites with  $V_{S30} > 800$  m/s and nine sites with  $V_{S30} > 1000$  m/s. As

TABLE 4

Smoothed  $\phi_{S25-mHV}$  and Smoothed  $R^2$  for Sites with and without Measured  $V_{S30}$ 

Period (s)	ASK14 and SWUS		With $V_{S30}$ Measurement			Without $V_{S30}$ Measurement			
	$\phi_{S25}$		Smoothed	$\phi_{S25-mHV1}$		Smoothed	$\phi_{S25-mHV2}$		$\phi_{VS30}$
	M 5	M 7	$R_1^2$	M 5	M 7	$R_2^2$	M 5	M 7	
0.05	0.578	0.376	0.000	0.578	0.376	0.000	0.611	0.425	0.199
0.1	0.581	0.386	0.000	0.581	0.386	0.000	0.623	0.447	0.225
0.15	0.562	0.370	0.000	0.562	0.370	0.000	0.639	0.479	0.305
0.2	0.546	0.359	0.043	0.534	0.351	0.050	0.624	0.479	0.335
0.25	0.530	0.354	0.076	0.509	0.340	0.089	0.611	0.481	0.358
0.3	0.511	0.360	0.104	0.484	0.341	0.120	0.597	0.491	0.380
0.4	0.483	0.363	0.147	0.447	0.335	0.170	0.571	0.492	0.400
0.5	0.470	0.372	0.180	0.426	0.336	0.209	0.557	0.495	0.414
0.75	0.448	0.390	0.188	0.404	0.352	0.280	0.522	0.487	0.421
1	0.442	0.411	0.193	0.397	0.369	0.330	0.500	0.482	0.422
1.5	0.424	0.422	0.201	0.379	0.377	0.400	0.473	0.472	0.440
2	0.414	0.436	0.207	0.369	0.388	0.437	0.440	0.452	0.416
3	0.400	0.419	0.214	0.355	0.371	0.488	0.407	0.416	0.404
4	0.375	0.402	0.220	0.331	0.355	0.525	0.380	0.393	0.404

SWUS, southwestern U.S.

TABLE 5

Example of the Horizontal-to-Vertical Spectral Ratio (HVS $R^*(T)$ ) and Mean  $\delta S2S$  for Two Sites

Period (s)	Site 1		Site 2	
	ln(HVS $R^*$ )	Mean $\delta S2S$	ln(HVS $R^*$ )	Mean $\delta S2S$
0.050	-0.461	0.000	-0.339	0.000
0.100	0.247	0.000	-0.518	0.000
0.150	-0.128	-0.119	-0.386	-0.223
0.200	-0.200	-0.222	0.003	-0.130
0.250	0.009	-0.103	0.492	0.125
0.300	0.483	0.111	0.724	0.226
0.400	0.052	-0.105	0.829	0.269
0.500	0.011	-0.111	0.837	0.282
0.750	-0.301	-0.233	0.713	0.222
1.000	-0.248	-0.174	0.494	0.142
1.500	-0.579	-0.261	0.647	0.217
2.000	-0.507	-0.223	0.719	0.232
3.000	-0.367	-0.184	0.652	0.180
4.000	-0.348	-0.195	0.745	0.202

a result, the mHVS $R$  site factors are poorly constrained for hard rock sites. Developing constraints for site amplification for hard rock sites is difficult due to the small number of hard rock sites in empirical ground motion datasets. Microtremors at hard rock sites that have recordings from earthquakes should be measured to determine if mHVS $R$  provides a useful constraint on the site amplification at hard rock sites. We do not recommend using the current model at rock sites with  $V_{S30} > 1000$  m/s.

Even with these limitations, there is improved estimation of site amplification by including site-specific measurement of

mHVS $R$ . We believe that it is time to include site parameters from mHVS $R$  in future GMMs for California. In parallel, there is a need to develop standards for collecting mHVS $R$  at project sites for use with these new GMMs.

## DATA AND RESOURCES

The microtremors records were obtained through the ObsPy library of Python. The dataset of normalized horizontal-to-vertical spectral ratio (HVS $R$ ) and the ASK14 residuals are given in the supplemental material for each one of the 196 selected stations. The unpublished manuscript by V. Mercado, C. A. Pajaro, C. A. Arteta, F. Díaz, J. Montejo, M. Arcila, and N. Abrahamson (2021), "Semi-empirical model for estimation of the site amplification in northern South America," submitted to *Earthq. Spectra*.

## DECLARATION OF COMPETING INTERESTS

The authors acknowledge that there are no conflicts of interest recorded.

## ACKNOWLEDGMENTS

For this project, Camilo Pinilla was supported by the Jane Lewis Fellowship and funding from the U.S. Geological Survey. The authors thank Douglas Dreger and his research team from the Earth and Planetary Science department for providing assistance and advise on how to obtain the noise samples from the continuous recordings using the Python library ObsPy. The authors thank Olga Ktenidou, Adrian Rodriguez-Marek, Brady Cox, and Jonathan Stewart for providing helpful comments on the article.

## REFERENCES

Abrahamson, N., W. J. Silva, and R. Kamai (2014). Summary of the ASK14 ground motion relation for active crustal regions, *Earthq. Spectra* **30**, no. 3, 1025–1055.

- Al-Atik, L., N. Abrahamson, J. Bommer, F. Scherbaum, F. Cotton, and N. Kuehn (2010). The variability of ground-motion prediction models and its components, *Seismol. Res. Lett.* **81**, no. 5, 794–801.
- Ancheta, T., R. Darragh, J. P. Stewart, E. Seyhan, W. J. Silva, B. Chiou, K. Wooddell, R. W. Graves, A. Kottke, D. M. Boore, *et al.* (2014). NGA-West2 database, *Earthq. Spectra* **30**, no. 3, 989–1005.
- Arai, H., and K. Tokimatsu (2004). S-wave velocity profiling by inversion of microtremor H/V spectrum, *Bull. Seismol. Soc. Am.* **94**, no. 1, 53–63.
- Bonnefoy-Claudet, S., C. Cornou, P. Bard, F. Cotton, P. Moczo, J. Kristek, and D. Fäh (2006). H/V ratio: A tool for site effects evaluation. Results from 1-D noise simulations, *Geophys. J. Int.* **167**, 827–837.
- Boore, D., E. Thompson, and H. Cadet (2011). Regional correlations of VS30 and velocities averaged over depths less than and greater than 30 meters, *Bull. Seismol. Soc. Am.* **101**, 6, 3046–3059, doi: [10.1785/0120110071](https://doi.org/10.1785/0120110071).
- Bora, S., F. Scherbaum, N. Kuehn, and P. Stafford (2016). On the relationship between Fourier and response spectra: Implications for the adjustment of empirical ground-motion prediction equations (GMPEs), *Bull. Seismol. Soc. Am.* **106**, no. 3, 1235–1253.
- Bozorgnia, Y., N. Abrahamson, L. Al-Atik, T. Ancheta, G. Atkinson, J. Baker, A. Baltay, D. Boore, K. Campbell, B. Chiou, *et al.* (2014). NGA-West2 research project, *Earthq. Spectra* **30**, no. 3, 973, doi: [10.1193/072113EQS209M](https://doi.org/10.1193/072113EQS209M).
- Beyreuther, M., R. Barsch, L. Krischer, T. Megies, Y. Behr, and J. Wassermann (2010). ObsPy: A Python toolbox for seismology, *Seismol. Res. Lett.* **81**, no. 3, 530–533, doi: [10.1785/gssrl.81.3.530](https://doi.org/10.1785/gssrl.81.3.530).
- Cox, B. R., T. Cheng, J. P. Vantassel, and L. Manuel (2020). A statistical representation and frequency-domain window-rejection algorithm for single-station HVSR measurements, *Geophys. J. Int.* **221**, no. 3, 2170–2183.
- Cultrera, G., V. De Rubeis, N. Theodoulidis, H. Cadet, and P.Y. Bard (2014). Statistical correlation of earthquake and ambient noise spectral ratios, *Bull. Earthq. Eng.* **12**, 1493–1514.
- Di Alessandro, C., L. Bonilla, D. M. Boore, A. Rovelli, and O. Scotti (2012). Predominant-period site classification for response spectra prediction equations in Italy, *Bull. Seismol. Soc. Am.* **102**, no. 2, 680–695.
- Geopentech (2015). *Southwestern United States ground-motion characterization SSHAC level 3, Technical Report Rev. 2*, March 2015, Report to Pacific Gas & Electric.
- Ghofrani, H., G. M. Atkinson, and K. Goda (2013). Implications of the 2011 M 9.0 Tohoku Japan earthquake for the treatment of site effects in large earthquakes, *Bull. Earthq. Eng.* **11**, 171–203.
- Haghshenas, E., P.-Y. Bard, N. Theodoulidis, and , and SESAME WP04 Team (2008). Empirical evaluation of microtremor H/V spectral ratio, *Bull. Earthq. Eng.* **6**, 75–108.
- Hallal, M. M., and B.R. Cox (2022). Comparison of state-of-the-art approaches used to account for spatial variability in 1d ground response analyses, *ASCE J. Geotech. Geoenviron. Eng.* **148**, no. 5, doi: [10.1061/\(ASCE\)GT.1943-5606.0002774](https://doi.org/10.1061/(ASCE)GT.1943-5606.0002774).
- Hassani, B., A. Young, G. Atkinson, T. Feng, and L. Meng (2019). Comparison of site dominant frequency from earthquake and microseismic data in California, *Bull. Seismol. Soc. Am.* **109**, no. 3, 1034–1040.
- Kawase, H., Y. Mori, and F. Nagashima (2018). Difference of horizontal-to-vertical spectral ratios of observed earthquakes and microtremors and its application to S-wave velocity inversion based on the diffuse field concept, *Earth Planets Space* **70**, doi: [10.1186/s40623-017-0766-4](https://doi.org/10.1186/s40623-017-0766-4).
- Kawase, H., F. Nagashima, K. Nakano, and Y. Mori (2018). Direct evaluation of S-wave amplification factors from microtremor H/V ratios: Double empirical corrections to “Nakamura” method, *Soil Dynam. Earthq. Eng.* **126**, 105,067.
- Kawase, H., F. J. Sánchez-Sesma, and S. Matsushima (2011). The optimal use of horizontal-to-vertical spectral ratios of earthquake motions for velocity inversions based on diffuse-field theory for plane waves, *Bull. Seismol. Soc. Am.* **101**, no. 5, 2001–2014.
- Konno, K., and T. Ohmachi (1998). Ground-motion characteristics estimated from spectral ratio between horizontal and vertical components of microtremors, *Bull. Seismol. Soc. Am.* **88**, no. 1, 228–241.
- Lachet, C., D. Hatzfeld, P.-Y. Bard, N. Theodoulidis, C. Papaioannou, and A. Savvaids (1996). Site effects and microzonation in the city of Thessaloniki (Greece), *Bull. Seismol. Soc. Am.* **86**, 1692–1703.
- Molnar, S., J. F. Cassidy, S. Castellaro, C. Cornou, H. Crow, J. A. Hunter, S. Matsushima, F. J. Sánchez-Sesma, and A. Yong (2016). Application of MHVSR for site characterization: State-of-the-art, *16th World Conf. on Earthquake, 16WCEE 2017, Paper Number 4946*, Santiago Chile, 9–13 January 2017.
- Molnar, S., A. Sirohey, J. Assaf, P.-Y. Bard, S. Castellaro, C. Cornou, B. Cox, B. Guillier, B. Hassani, H. Kawase, *et al.* (2022). A review of the microtremor horizontal-to-vertical spectral ratio (MHVSR) method, *J. Seismol* **26**, no. 4, 653–685, doi: [10.1007/s10950-021-10062-9](https://doi.org/10.1007/s10950-021-10062-9).
- Najafostomari, M., H. Rahimi, G. Tanircan, A. Babaie Mahani, and M. Shahvar (2020). Site Classification and probabilistic estimation of VS30 for the Iranian strong-motion network, *Phys. Earth Planet. Int.* **308**, 106,583.
- Nakamura, Y. (1989). A method for dynamic characteristics estimation of subsurface using microtremor on the ground surface, *Q. Rep. Railway. Tech. Res. Inst.* **30**, 25–33.
- Pinzón, L., L. Pujades, A. Macau, E. Carreño, and J. Alcalde (2019). Seismic site classification from the horizontal-to-vertical response spectral ratios: Use of the Spanish strong-motion database, *Geoscience* **9**, no. 7, 294.
- Pitilakis, K., E. Riga, A. Anastasiadis, S. Fotopoulou, and S. Karafagka (2018). Toward the revision of EC8: Proposal for an alternative site classification scheme and associated intensity dependent spectral amplification factors, *Soil Dynam. Earthq. Eng.* **126**, 105,137, doi: [10.1016/j.soildyn.2018.03.030](https://doi.org/10.1016/j.soildyn.2018.03.030).
- Rodriguez, V. H. S., and S. Midorikawa (2003). Comparison of spectral ratio techniques for estimation of site effects using microtremor data and earthquake motions recorded at the surface and in boreholes, *Earthq. Eng. Struct. Dynam.* **32**, 1691–1714.
- Senna, S., S. Midorikawa, and K. Wakamatsu (2008). Estimation of spectral amplification of ground using H/V spectral ratio of microtremors and geomorphological land classification, *J. Jpn. Assoc. Earthq. Eng.* **8**, 1–15.
- Teague, D. P., B. R. Cox, and E. R. Rathje (2018). Measured vs. predicted site response at the Garner valley downhole array considering shear wave velocity uncertainty from borehole and surface wave methods, *Soil Dynam. Earthq. Eng.* **113**, no. 10, 339–355, doi: [10.1016/j.soildyn.2018.05.031](https://doi.org/10.1016/j.soildyn.2018.05.031).

- Satoh, T., H. Kawase, and S. Matsushima (2001). Differences between site characteristics obtained from microtremors, S-waves, P-waves and codas, *Bull. Seismol. Soc. Am.* **91**, no. 2, 313–334.
- Site EffectS Assessment using Ambient Excitations (SESAME) (2004). Guidelines for the implementation of the H/V spectral ratio technique on ambient vibrations measurements, processing, and interpretation, Research General Directorate, 62, European Commission—Research General Directorate.
- Standards New Zealand (SNZ) (2004). Structural design actions. Part 5: Earthquake actions—New Zealand, NZS 1170.5:2004, SNZ, Wellington, New Zealand.
- Wang, P., P. Zimmaro, T. Gospe, S. K. Ahdi, A. Yong, and J. P. Stewart (2021). Horizontal-to-vertical spectral ratios from California sites: Open-source database and data interpretation to establish site parameters, *Report GIRS-2021-06*, B. John Garrick Risk Institute, Natural Hazards Risk and Resiliency Research Center, UCLA, 64 pp, doi: [10.34948/N3KW20](https://doi.org/10.34948/N3KW20).
- Working Group on California Earthquake Probabilities (2003). *Earthquake probabilities in the San Francisco Bay region: 2002–2031*, U.S. Geol. Surv. Open-File Rept. 2003-214.
- Zhao, J. X., K. Irikura, J. Zhang, Y. Fukushima, P. G. Somerville, A. Asano, Y. Ohno, T. Oouchi, T. Takahashi, and H. Ogawa (2006). An empirical site-classification method for strong-motion stations in Japan using H/V response spectral ratio, *Bull. Seismol. Soc. Am.* **96**, no. 3, 914–925.

---

Manuscript received 5 March 2022

Published online 18 October 2022